3D proton structure in momentum space

Valerio Bertone

IRFU, CEA, Université Paris-Saclay

October 24, 2023, Forward physics and QCD at the LHC and EIC, Bad Honnef

This project has received funding from the European Union's Horizon 2020 research and innovation programme under grant agreement № 824093

Introduction

- The **transverse momentum** (q_{T}) distribution of a **high-mass** (Q) system has two main regimes:
  - for $q_{\mathrm{T}} \gtrsim \mathrm{Q}$ **collinear factorisation** at *fixed perturbative order* is appropriate:

$$\left(\frac{d\sigma}{dq_T}\right)_{\text{f.o.}} = \int_0^1 dx_1 \int_0^1 dx_2 f_1(x_1, Q) f_2(x_2, Q) \frac{d\hat{\sigma}}{dq_T} + \mathcal{O}\left[\left(\frac{\Lambda_{\mathrm{QCD}}}{Q}\right)^n\right]$$

  - for $q_{\mathrm{T}} \ll \mathrm{Q}$ **transverse-momentum-dependent (TMD) factorisation** at *fixed logarithmic order* is appropriate:

$$\left(\frac{d\sigma}{dq_T}\right)_{\text{res.}} \overset{\text{TMD}}{=} \sigma_0 H(Q) \int d^2\mathbf{b}_T e^{i\mathbf{b}_T\cdot\mathbf{q}_T} F_1(x_1, \mathbf{b}_T, Q, Q^2) F_2(x_2, \mathbf{b}_T, Q, Q^2) + \mathcal{O}\left[\left(\frac{q_T}{Q}\right)^m\right]$$

  - Collinear and TMD factorisations may eventually be **matched** to produce accurate results over the the full q_{T} spectrum.

Introduction

- The **transverse momentum** (q_{T}) distribution of a **high-mass** (Q) system has two main regimes:
  - for $q_{\mathrm{T}} \gtrsim \mathrm{Q}$ **collinear factorisation** at *fixed perturbative order* is appropriate:

$$\left(\frac{d\sigma}{dq_T}\right)_{\text{f.o.}} = \int_0^1 dx_1 \int_0^1 dx_2 f_1(x_1, Q) f_2(x_2, Q) \frac{d\hat{\sigma}}{dq_T} + \mathcal{O}\left[\left(\frac{\Lambda_{\mathrm{QCD}}}{Q}\right)^n\right]$$

  - for $q_{\mathrm{T}} \ll \mathrm{Q}$ **transverse-momentum-dependent (TMD) factorisation** at *fixed logarithmic order* is appropriate:

Main subject of this talk

$$\left(\frac{d\sigma}{dq_T}\right)_{\text{res.}} \overset{\text{TMD}}{=} \sigma_0 H(Q) \int d^2\mathbf{b}_T e^{i\mathbf{b}_T\cdot\mathbf{q}_T} F_1(x_1, \mathbf{b}_T, Q, Q^2) F_2(x_2, \mathbf{b}_T, Q, Q^2) + \mathcal{O}\left[\left(\frac{q_T}{Q}\right)^m\right]$$

- Collinear and TMD factorisations may eventually be **matched** to produce accurate results over the the full q_{T} spectrum.

TMD factorisation

- TMD factorisation introduces two independent scales:
  - the **renormalisation scale μ**, originating from the UV renormalisation,
  - the **rapidity scale ζ**, originating from the cancellation of rapidity divergences.
- The respective **evolution equations** are:

$$\frac{\partial \ln F}{\partial \ln \sqrt{\zeta}} = K(\mu_0) - \int_{\mu_0}^{\mu} \frac{d\mu'}{\mu'} \gamma_K(\alpha_s(\mu'))$$

$$\frac{\partial \ln F}{\partial \ln \mu} = \gamma_F(\alpha_s(\mu)) - \gamma_K(\alpha_s(\mu)) \ln \frac{\sqrt{\zeta}}{\mu}$$

- At small b_T, TMDs can be matched onto collinear distributions:

$$F(\mu, \zeta) = C(\mu, \zeta) \otimes f(\mu)$$

- The solution final is:

$$F(\mu,\zeta) = \exp\left\{ K(\mu_0) \ln \frac{\sqrt{\zeta}}{\sqrt{\zeta_0}} + \int_{\mu_0}^{\mu} \frac{d\mu'}{\mu'} \left[\gamma_F(\alpha_s(\mu')) - \gamma_K(\alpha_s(\mu')) \ln \frac{\sqrt{\zeta}}{\mu'} \right] \right\} C(\mu_0, \zeta_0) \otimes f(\mu_0)$$

- Anomalous dims. and matching funcs. **perturbatively** computable.

TMD factorisation

- TMD factorisation introduces two independent scales:
  - the **renormalisation scale μ**, originating from the UV renormalisation,
  - the **rapidity scale ζ**, originating from the cancellation of rapidity divergences.
- The respective **evolution equations** are:

$$\frac{\partial \ln F}{\partial \ln \sqrt{\zeta}} = K(\mu_0) - \int_{\mu_0}^{\mu} \frac{d\mu'}{\mu'} \gamma_K(\alpha_s(\mu'))$$

$$\frac{\partial \ln F}{\partial \ln \mu} = \gamma_F(\alpha_s(\mu)) - \gamma_K(\alpha_s(\mu)) \ln \frac{\sqrt{\zeta}}{\mu}$$

- At small b_T, TMDs can be matched onto collinear distributions:

$$F(\mu, \zeta) = C(\mu, \zeta) \otimes f(\mu)$$

- The solution final is:

$\mu_b = b_0 / b_T$

$$F(\mu, \zeta) = \exp\left\{ K(\mu_0) \ln \frac{\sqrt{\zeta}}{\sqrt{\zeta_0}} + \int_{\mu_0}^{\mu} \frac{d\mu'}{\mu'} \left[\gamma_F(\alpha_s(\mu')) - \gamma_K(\alpha_s(\mu')) \ln \frac{\sqrt{\zeta}}{\mu'} \right] \right\} C(\mu_0, \zeta_0) \otimes f(\mu_0)$$

- Anomalous dims. and matching funcs. **perturbatively** computable.

TMD factorisation

- When integrating over b_T, **large values of** b_T give raise to low scales in the **non-perturbative** region.

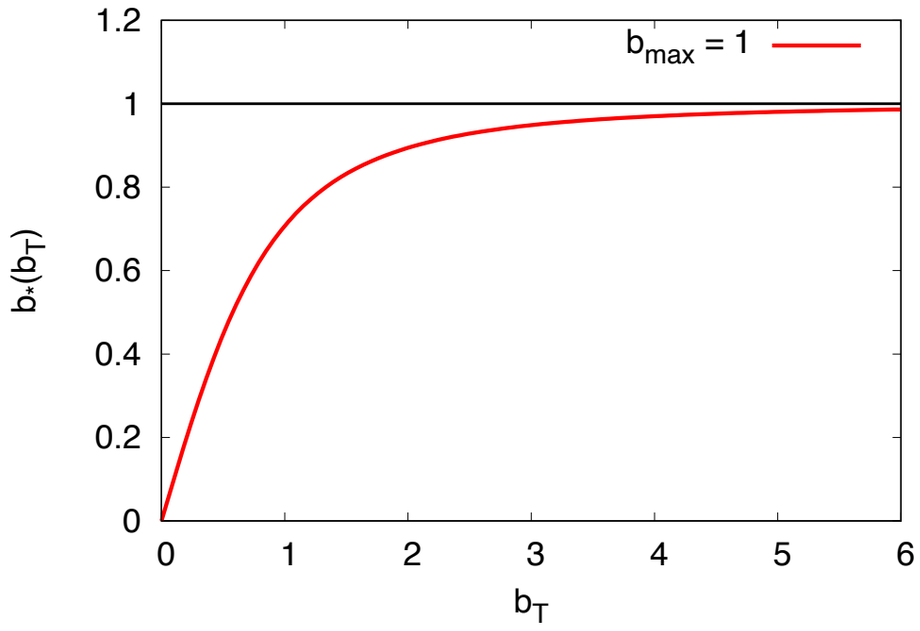

- Introduce the so-called **b*-prescription**:

$$b_*(b_T) = \frac{b_T}{\sqrt{1 + b_T^2/b_{\rm max}^2}}$$

- and rewrite:

$$F(x, b_T, \mu, \zeta) = \left[\frac{F(x, b_T, \mu, \zeta)}{F(x, b_*(b_T), \mu, \zeta)}\right] F(x, b_*(b_T), \mu, \zeta) \equiv f_{\rm NP}(x, b_T, \zeta) F(x, b_*(b_T), \mu, \zeta)$$

TMD factorisation

- When integrating over b_T, **large values of** b_T give raise to low scales in the **non-perturbative** region.

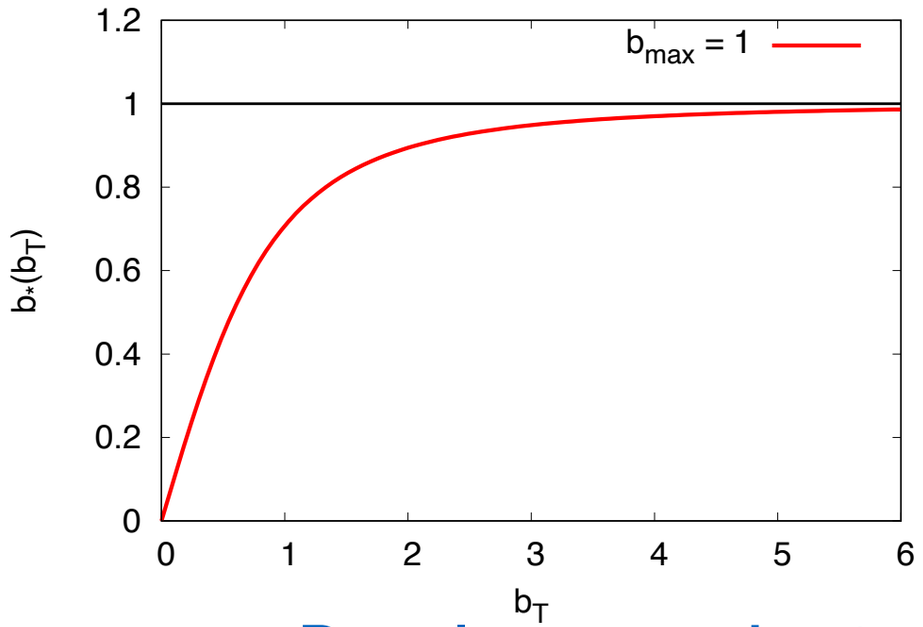

- Introduce the so-called **b*-prescription**:

$$b_*(b_T) = \frac{b_T}{\sqrt{1 + b_T^2/b_{\max}^2}}$$

- and rewrite:

Purely perturbative

$$F(x, b_T, \mu, \zeta) = \left[\frac{F(x, b_T, \mu, \zeta)}{F(x, b_*(b_T), \mu, \zeta)}\right] F(x, b_*(b_T), \mu, \zeta) \equiv f_{\rm NP}(x, b_T, \zeta) F(x, b_*(b_T), \mu, \zeta)$$

Non-perturbative, determine from data

- Properties of $f_{\rm NP}$:
  - has to go to **one** as b_T goes to zero: reproduce the fully perturbative regime,
  - has to got to **zero** as b_T becomes large: mimic the Sudakov suppression.
- Bottom line: avoidance of the non-perturbative region upon integration in b_T implies the presence of **both** b_*-prescription and $f_{\rm NP}$.

TMD factorisation

- Final expression:

$$F_{f/P}(x, \mathbf{b}_T; \mu, \zeta) = \sum_j C_{f/j}(x, b_*; \mu_b, \mu_b^2) \otimes f_{j/P}(x, \mu_b) \quad : A$$

$$\times \exp\left\{ K(b_*; \mu_b) \ln \frac{\sqrt{\zeta}}{\mu_b} + \int_{\mu_b}^{\mu} \frac{d\mu'}{\mu'} \left[\gamma_F - \gamma_K \ln \frac{\sqrt{\zeta}}{\mu'} \right] \right\} \quad : B$$

$$\times \exp\left\{ g_{j/P}(x, b_T) + g_K(b_T) \ln \frac{\sqrt{\zeta_F}}{\sqrt{\zeta_{F,0}}} \right\} \quad : C$$

TMD factorisation

- Final expression:

$$F_{f/P}(x, \mathbf{b}_T; \mu, \zeta) = \sum_j C_{f/j}(x, b_*; \mu_b, \mu_b^2) \otimes f_{j/P}(x, \mu_b) \qquad : A$$

$$\times \quad \exp\left\{ K(b_*; \mu_b) \ln \frac{\sqrt{\zeta}}{\mu_b} + \int_{\mu_b}^{\mu} \frac{d\mu'}{\mu'} \left[\gamma_F - \gamma_K \ln \frac{\sqrt{\zeta}}{\mu'} \right] \right\} \qquad : B$$

$$\times \quad \exp\left\{ g_{j/P}(x, b_T) + g_K(b_T) \ln \frac{\sqrt{\zeta_F}}{\sqrt{\zeta_{F,0}}} \right\} \qquad : C$$

- matching onto the collinear region at $b_\mathrm{T} \ll 1/\Lambda_\mathrm{QCD}$,
- factorises as *hard* (perturbative) and *longitudinal* (*i.e.* collinear, non-perturbative).

TMD factorisation

- Final expression:

$$F_{f/P}(x, \mathbf{b}_T; \mu, \zeta) = \sum_j C_{f/j}(x, b_*; \mu_b, \mu_b^2) \otimes f_{j/P}(x, \mu_b) \quad : A$$

$$\times \exp\left\{ K(b_*; \mu_b) \ln \frac{\sqrt{\zeta}}{\mu_b} + \int_{\mu_b}^{\mu} \frac{d\mu'}{\mu'} \left[\gamma_F - \gamma_K \ln \frac{\sqrt{\zeta}}{\mu'} \right] \right\} \quad : B$$

$$\times \exp\left\{ g_{j/P}(x, b_T) + g_K(b_T) \ln \frac{\sqrt{\zeta_F}}{\sqrt{\zeta_{F,0}}} \right\} \quad : C$$

- matching onto the collinear region at $b_\mathrm{T} \ll 1/\Lambda_\mathrm{QCD}$,
- factorises as *hard* (perturbative) and *longitudinal* (*i.e.* collinear, non-perturbative).

- CS and RGE evolution,
- evolution in μ and ζ,
- perturbative.

TMD factorisation

- Final expression:

$$F_{f/P}(x, \mathbf{b}_T; \mu, \zeta) = \sum_j C_{f/j}(x, b_*; \mu_b, \mu_b^2) \otimes f_{j/P}(x, \mu_b) \quad : A$$

$$\times \exp\left\{ K(b_*; \mu_b) \ln \frac{\sqrt{\zeta}}{\mu_b} + \int_{\mu_b}^{\mu} \frac{d\mu'}{\mu'} \left[\gamma_F - \gamma_K \ln \frac{\sqrt{\zeta}}{\mu'} \right] \right\} \quad : B$$

$$\times \exp\left\{ g_{j/P}(x, b_T) + g_K(b_T) \ln \frac{\sqrt{\zeta_F}}{\sqrt{\zeta_{F,0}}} \right\} \quad : C$$

- matching onto the collinear region at $b_\mathrm{T} \ll 1/\Lambda_\mathrm{QCD}$,
- factorises as *hard* (perturbative) and *longitudinal* (*i.e.* collinear, non-perturbative).
  - avoid the Landau pole,
  - f_NP accounts for the introduction of b_*,
  - f_NP is non-perturbative thus **fit** to data.
- CS and RGE evolution,
- evolution in μ and ζ,
- perturbative.

Factorising processes

- Processes for which leading-power TMD factorisation has been **proven**:

Drell-Yan

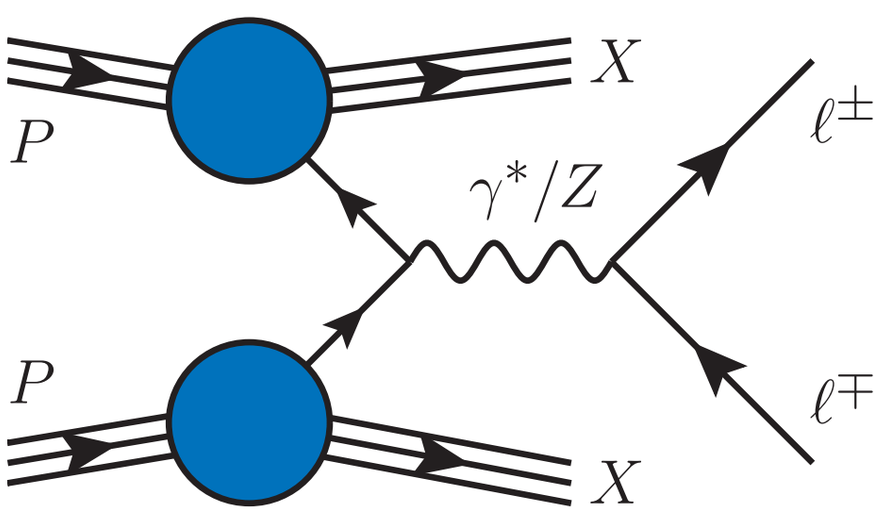

$$P P \longrightarrow \ell^\pm \ell^\mp \, X$$

- **Two** TMD **PDFs**:
- Lots of data:
  - low-energy: FNAL,
  - mid-energy: RHIC,
  - high-energy: Tevatron, LHC.

Semi-inclusive DIS

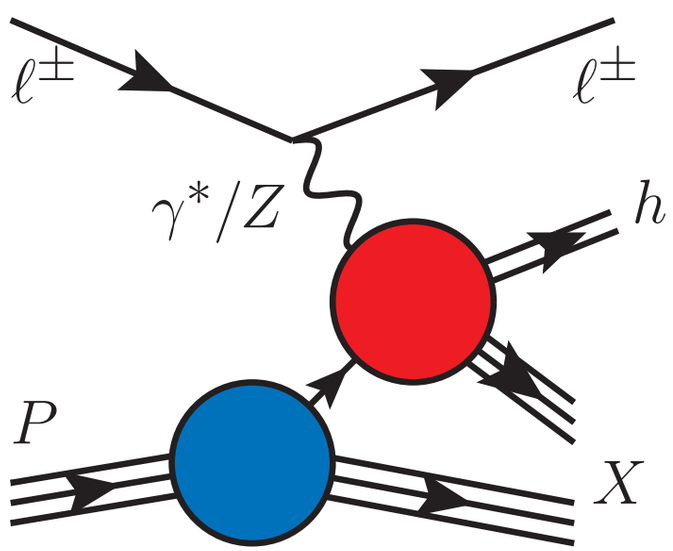

$$P \ell^\pm \longrightarrow \ell^\pm h \, X$$

- One TMD **PDF** one **FF**:
- many precise data points:
  - HERMES at DESY,
  - COMPASS at CERN.

e^+e^- annihilation

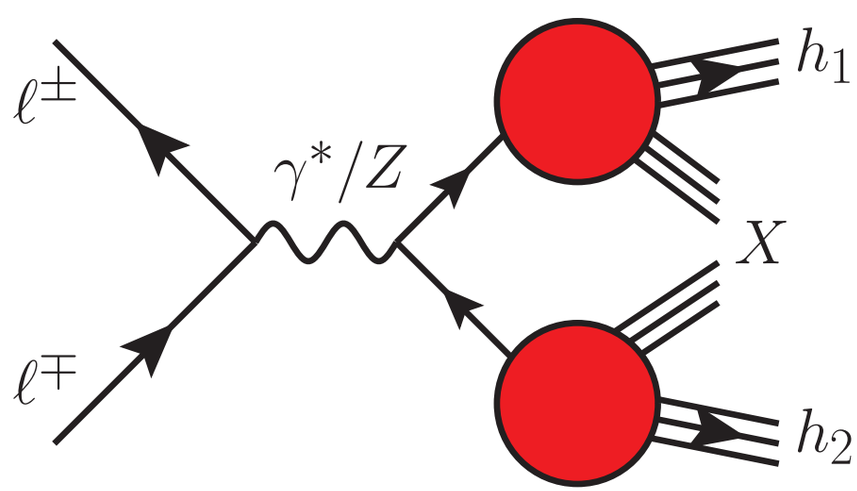

$$\ell^\pm \ell^\mp \to h_1 h_2 \, X$$

- **Two** TMD **FFs**:
- di-hadron prod. from:
  - BELLE at KEK,
  - BABAR at SLAC.

- Examples of other precesses:
  - thrust and p_{hT} distributions in single-hadron production in e^+e^-,
  - hadron-in-jet production,
  - …

Logarithmic counting

$$\left(\frac{d\sigma}{dq_T}\right)_{\text{res.}} \overset{\text{TMD}}{=} \sigma_0 H(Q) \int d^2\mathbf{b}_T e^{i\mathbf{b}_T\cdot\mathbf{q}_T} F_1(x_1,\mathbf{b}_T,Q,Q^2) F_2(x_2,\mathbf{b}_T,Q,Q^2)$$

$$F_i = \sum_j \left(C_{i/j}\otimes f_j\right) \exp\left\{K\,\ln\frac{\sqrt{\zeta}}{\mu_b} + \int_{\mu_b}^{\mu}\frac{d\mu'}{\mu'}\left[\gamma_F - \gamma_K \ln\frac{\sqrt{\zeta}}{\mu'}\right]\right\}$$

Accuracy	γ_K	γ_F	K	$C_{f/j}$	H	FFs/PDFs/α_s
LL	α_s	-	-	1	1	-
NLL	α_s^2	α_s	α_s	1	1	LO
NLL’	α_s^2	α_s	α_s	α_s	α_s	LO
N^{2}LL	α_s^3	α_s^2	α_s^2	α_s	α_s	NLO
N^{2}LL’	α_s^3	α_s^2	α_s^2	α_s^2	α_s^2	NLO
N^{3}LL	α_s^4	α_s^3	α_s^3	α_s^2	α_s^2	NNLO
N^{3}LL’	α_s^4	α_s^3	α_s^3	α_s^3	α_s^3	NNLO

Perturbative convergence

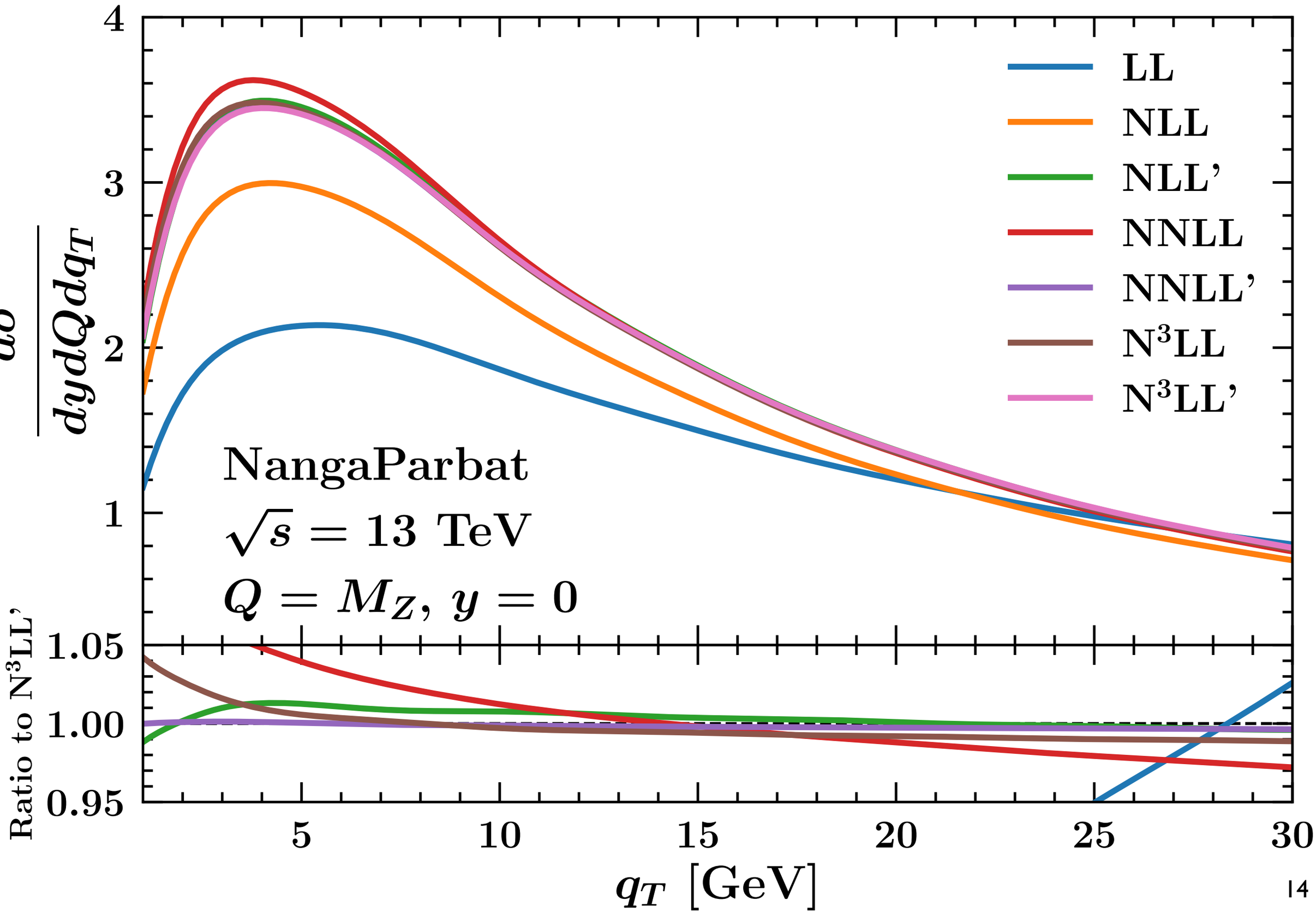

TMD, q_T resummation, SCET

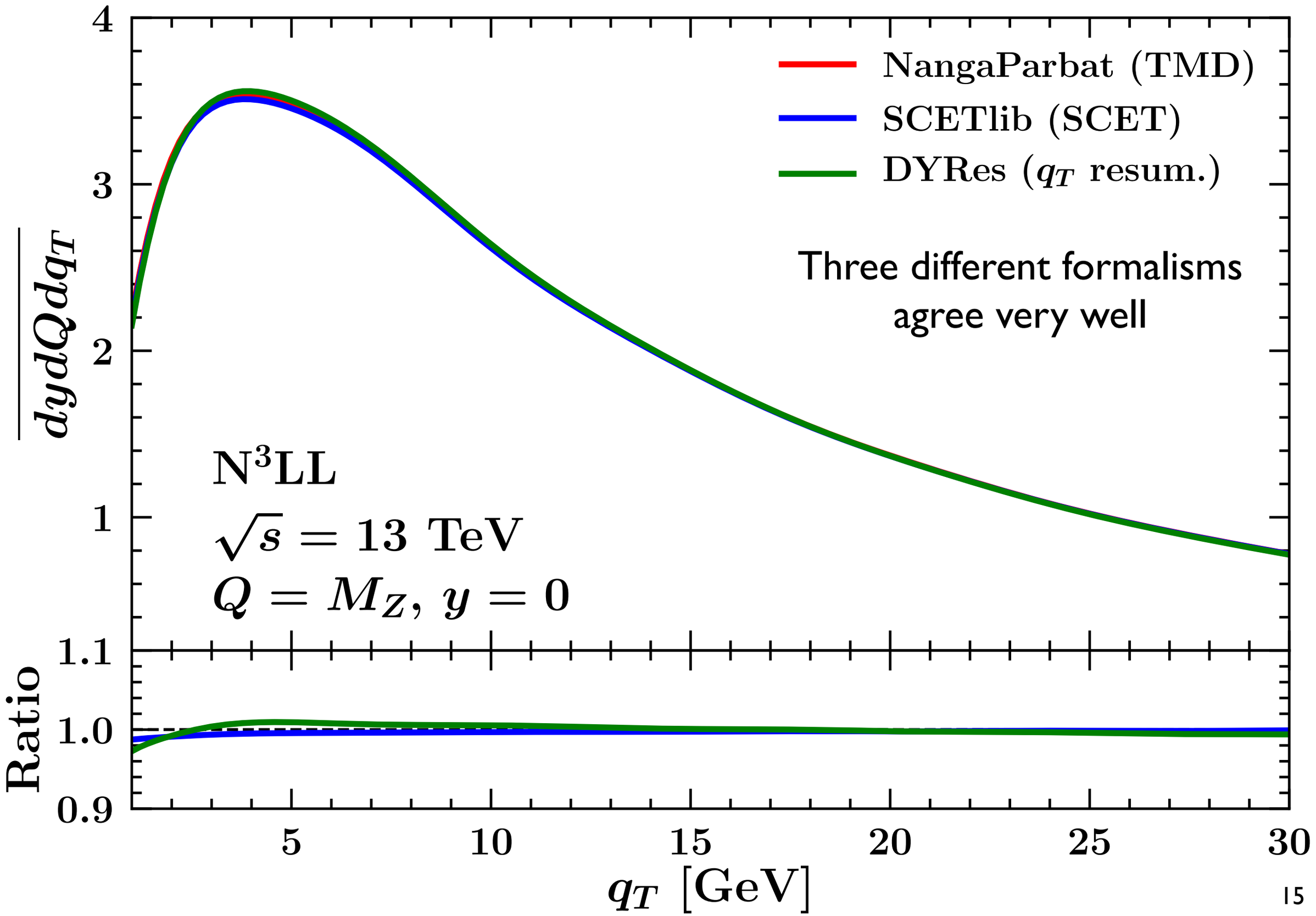

Unpolarised TMD extractions

A selection of fits

	Accuracy	SIDIS	Drell-Yan	N. of points
DWS 1984, CERN-TH.3987/84	NLL	✘	✔	a few
BLNY 2003, hep-ph/0212159	NLL'-NNLL	✘	✔	116
Pavia 2013, 1309.3507	No evolution	✔	✘	1538 (HERMES)
Torino 2014, 1312.6261	No evolution	✔	✘	576 (H) 6284 (C)
DEMS 2014, 1407.3311	NNLL	✘	✔	223
Pavia 2017, 1703.10157	NLL	✔	✔	8059
SV 2017, 1706.01473	N^3LL	✘	✔ (LHC)	309
BSV 2019, 1902.08474	N^3LL	✘	✔ (LHC)	457
SV 2019,1912.06532	$N^3LL^{(-)}$	✔	✔ (LHC)	1039
Pavia 2019, 1912.07550	N^3LL	✘	✔ (LHC)	353
SV+ 2022, 2201.07114	N^3LL	✘	✔ (LHC)	507/309
MAPTMD 2022, 2206.07598	$N^3LL^{(-)}$	✔	✔ (LHC)	2031

Unpolarised TMD extractions

A selection of fits

	Accuracy	SIDIS	Drell-Yan	N. of points
DWS 1984, CERN-TH.3987/84	NLL	✘	✔	a few
BLNY 2003, hep-ph/0212159	NLL'-NNLL	✘	✔	116
Pavia 2013, 1309.3507	No evolution	✔	✘	1538 (HERMES)
Torino 2014, 1312.6261	No evolution	✔	✘	576 (H) 6284 (C)
DEMS 2014, 1407.3311	NNLL	✘	✔	223
Pavia 2017, 1703.10157	NLL	✔	✔	8059
SV 2017, 1706.01473	N^3LL	✘	✔ (LHC)	309
BSV 2019, 1902.08474	N^3LL	✘	✔ (LHC)	457
SV 2019,1912.06532	$N^3LL^{(-)}$	✔	✔ (LHC)	1039
Pavia 2019, 1912.07550	N^3LL	✘	✔ (LHC)	353
SV+ 2022, 2201.07114	N^3LL	✘	✔ (LHC)	507/309
MAPTMD 2022, 2206.07598	$N^3LL^{(-)}$	✔	✔ (LHC)	2031

Unpolarised TMD extractions

Many more studies and extractions…

- TMD fragmentation functions from e^+e^- data [2108.04182, 1704.08882]
- W production in pp collisions [2011.05351]
- Di-jet and heavy-meson pair production in DIS [2008.07531, 2111.03703]
- Dijet production in pp collisions [*e.g.* 1807.07573]
- hadron-in-jet production [1612.04817]
- Model-independent prescription to extract TMDs [2201.07237]
- Parton-branching methods [*e.g.* 1804.11152]
- q_T-resummation based extractions [2203.05394]
- Study of the Sivers TMDs [1308.5003, 2004.14278, 2009.10710, 2103.03270,...]
- Pion TMDs [1907.10356, 2210.01733]
- TMD flavour dependence [1807.02101, 2201.07114]
- …

MAPTMD 2022

Main settings

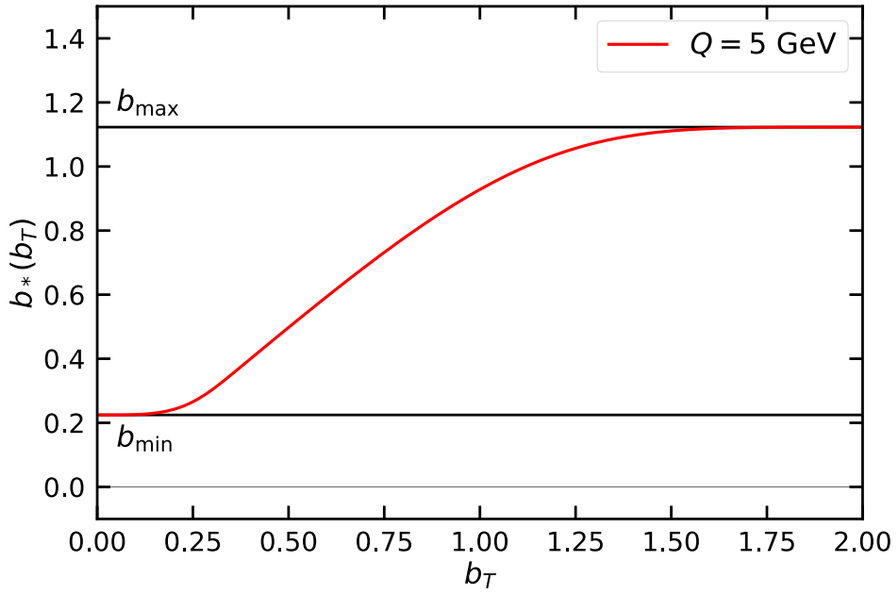

- $b*$ prescription:

$$b_*(b_T) = b_{\max}\left(\frac{1-e^{-b_T^4/b_{\max}^4}}{1-e^{-b_T^4/b_{\min}^4}}\right)^{1/4} \quad \text{with} \quad \begin{cases} b_{\max} = 2e^{-\gamma_E} \\ b_{\min} = b_{\max}/Q \end{cases}$$

- Non-perturbative function $f_{\rm NP}$:
  - evolution (CS kernel): $g_K(\boldsymbol{b}_T^2) = -g_2^2\,\dfrac{\boldsymbol{b}_T^2}{2}$
  - PDFs:

$$f_{1\,NP}(x,\boldsymbol{b}_T^2;\zeta,Q_0) = \frac{g_1(x)\,e^{-g_1(x)\frac{\boldsymbol{b}_T^2}{4}} + \lambda^2\,g_{1B}^2(x)\left[1-g_{1B}(x)\frac{\boldsymbol{b}_T^2}{4}\right]e^{-g_{1B}(x)\frac{\boldsymbol{b}_T^2}{4}} + \lambda_2^2\,g_{1C}(x)\,e^{-g_{1C}(x)\frac{\boldsymbol{b}_T^2}{4}}}{g_1(x)+\lambda^2\,g_{1B}^2(x)+\lambda_2^2\,g_{1C}(x)}\left[\frac{\zeta}{Q_0^2}\right]^{g_K(\boldsymbol{b}_T^2)/2}$$

  - FFs:

$$D_{1\,NP}(z,\boldsymbol{b}_T^2;\zeta,Q_0) = \frac{g_3(z)\,e^{-g_3(z)\frac{\boldsymbol{b}_T^2}{4z^2}} + \frac{\lambda_F}{z^2}\,g_{3B}^2(z)\left[1-g_{3B}(z)\frac{\boldsymbol{b}_T^2}{4z^2}\right]e^{-g_{3B}(z)\frac{\boldsymbol{b}_T^2}{4z^2}}}{g_3(z)+\frac{\lambda_F}{z^2}\,g_{3B}^2(z)}\left[\frac{\zeta}{Q_0^2}\right]^{g_K(\boldsymbol{b}_T^2)/2}$$

$$g_{\{1,1B,1C\}}(x) = N_{\{1,1B,1C\}}\frac{x^{\sigma_{\{1,2,3\}}}(1-x)^{\alpha^2_{\{1,2,3\}}}}{\hat{x}^{\sigma_{\{1,2,3\}}}(1-\hat{x})^{\alpha^2_{\{1,2,3\}}}} \qquad g_{\{3,3B\}}(z) = N_{\{3,3B\}}\frac{(z^{\beta_{\{1,2\}}}+\delta^2_{\{1,2\}})(1-z)^{\gamma^2_{\{1,2\}}}}{(\hat{z}^{\beta_{\{1,2\}}}+\delta^2_{\{1,2\}})(1-\hat{z})^{\gamma^2_{\{1,2\}}}}$$

- 11 (PDFs) + 9 (FFs) + 1 (evol): **21 free parameters** to fit to data.
- Perturbative accuracies: **N³LL(-)**.
- **Monte Carlo** method for the experimental error propagation.

MAPTMD 2022

Dataset

- DY data:
  - fixed-target low-energy DY,
  - RHIC data,
  - LHC and Tevatron data,
  - selection cut q_T / $Q < 0.2$,
  - 484 data points.
- SIDIS data:
  - HERMES and COMPASS,
  - $P_{hT}|_{\max} = \min[\min[0.2Q, 0.5zQ] + 0.3 \text{ GeV}, zQ]$
  - $Q > 1.4$ GeV, $0.2 < z < 0.7$,
  - 1547 points.

Experiment	$N_{\rm dat}$	Observable	$\sqrt{s}$ [GeV]	Q [GeV]	y or x_F	Lepton cuts	Ref.
E605	50	$Ed^3\sigma/d^3\boldsymbol{q}$	38.8	7 - 18	$x_F = 0.1$	-	[55]
E772	53	$Ed^3\sigma/d^3\boldsymbol{q}$	38.8	5 - 15	$0.1 < x_F < 0.3$	-	[51]
E288 200 GeV	30	$Ed^3\sigma/d^3\boldsymbol{q}$	19.4	4 - 9	$y = 0.40$	-	[56]
E288 300 GeV	39	$Ed^3\sigma/d^3\boldsymbol{q}$	23.8	4 - 12	$y = 0.21$	-	[56]
E288 400 GeV	61	$Ed^3\sigma/d^3\boldsymbol{q}$	27.4	5 - 14	$y = 0.03$	-	[56]
STAR 510	7	$d\sigma/d\lvert\boldsymbol{q}_T\rvert$	510	73 - 114	$\lvert y\rvert < 1$	$p_{T\ell} > 25$ GeV $\lvert\eta_\ell\rvert < 1$	-
PHENIX200	2	$d\sigma/d\lvert\boldsymbol{q}_T\rvert$	200	4.8 - 8.2	$1.2 < y < 2.2$	-	[52]
CDF Run I	25	$d\sigma/d\lvert\boldsymbol{q}_T\rvert$	1800	66 - 116	Inclusive	-	[57]
CDF Run II	26	$d\sigma/d\lvert\boldsymbol{q}_T\rvert$	1960	66 - 116	Inclusive	-	[58]
D0 Run I	12	$d\sigma/d\lvert\boldsymbol{q}_T\rvert$	1800	75 - 105	Inclusive	-	[59]
D0 Run II	5	$(1/\sigma)d\sigma/d\lvert\boldsymbol{q}_T\rvert$	1960	70 - 110	Inclusive	-	[60]
D0 Run II (μ)	3	$(1/\sigma)d\sigma/d\lvert\boldsymbol{q}_T\rvert$	1960	65 - 115	$\lvert y\rvert < 1.7$	$p_{T\ell} > 15$ GeV $\lvert\eta_\ell\rvert < 1.7$	[61]
LHCb 7 TeV	7	$d\sigma/d\lvert\boldsymbol{q}_T\rvert$	7000	60 - 120	$2 < y < 4.5$	$p_{T\ell} > 20$ GeV $2 < \eta_\ell < 4.5$	[62]
LHCb 8 TeV	7	$d\sigma/d\lvert\boldsymbol{q}_T\rvert$	8000	60 - 120	$2 < y < 4.5$	$p_{T\ell} > 20$ GeV $2 < \eta_\ell < 4.5$	[63]
LHCb 13 TeV	7	$d\sigma/d\lvert\boldsymbol{q}_T\rvert$	13000	60 - 120	$2 < y < 4.5$	$p_{T\ell} > 20$ GeV $2 < \eta_\ell < 4.5$	[64]
CMS 7 TeV	4	$(1/\sigma)d\sigma/d\lvert\boldsymbol{q}_T\rvert$	7000	60 - 120	$\lvert y\rvert < 2.1$	$p_{T\ell} > 20$ GeV $\lvert\eta_\ell\rvert < 2.1$	[65]
CMS 8 TeV	4	$(1/\sigma)d\sigma/d\lvert\boldsymbol{q}_T\rvert$	8000	60 - 120	$\lvert y\rvert < 2.1$	$p_{T\ell} > 15$ GeV $\lvert\eta_\ell\rvert < 2.1$	[66]
CMS 13 TeV	70	$d\sigma/d\lvert\boldsymbol{q}_T\rvert$	13000	76 - 106	$\lvert y\rvert < 0.4$ $0.4 < \lvert y\rvert < 0.8$ $0.8 < \lvert y\rvert < 1.2$ $1.2 < \lvert y\rvert < 1.6$ $1.6 < \lvert y\rvert < 2.4$	$p_{T\ell} > 25$ GeV $\lvert\eta_\ell\rvert < 2.4$	[53]
ATLAS 7 TeV	6 6 6	$(1/\sigma)d\sigma/d\lvert\boldsymbol{q}_T\rvert$	7000	66 - 116	$\lvert y\rvert < 1$ $1 < \lvert y\rvert < 2$ $2 < \lvert y\rvert < 2.4$	$p_{T\ell} > 20$ GeV $\lvert\eta_\ell\rvert < 2.4$	[67]
ATLAS 8 TeV on-peak	6 6 6 6 6 6	$(1/\sigma)d\sigma/d\lvert\boldsymbol{q}_T\rvert$	8000	66 - 116	$\lvert y\rvert < 0.4$ $0.4 < \lvert y\rvert < 0.8$ $0.8 < \lvert y\rvert < 1.2$ $1.2 < \lvert y\rvert < 1.6$ $1.6 < \lvert y\rvert < 2$ $2 < \lvert y\rvert < 2.4$	$p_{T\ell} > 20$ GeV $\lvert\eta_\ell\rvert < 2.4$	[68]
ATLAS 8 TeV off-peak	4 8	$(1/\sigma)d\sigma/d\lvert\boldsymbol{q}_T\rvert$	8000	46 - 66 116 - 150	$\lvert y\rvert < 2.4$	$p_{T\ell} > 20$ GeV $\lvert\eta_\ell\rvert < 2.4$	[68]
ATLAS 13 TeV	6	$(1/\sigma)d\sigma/d\lvert\boldsymbol{q}_T\rvert$	13000	66 - 113	$\lvert y\rvert < 2.5$	$p_{T\ell} > 27$ GeV $\lvert\eta_\ell\rvert < 2.5$	[54]
Total	484						

Experiment	$N_{\rm dat}$	Observable	Channels	Q [GeV]	x	z	Phase space cuts	Ref.
HERMES	344	$M(x, z, \lvert\boldsymbol{P}_{hT}\rvert, Q)$	$p \to \pi^+$ $p \to \pi^-$ $p \to K^+$ $p \to K^-$ $d \to \pi^+$ $d \to \pi^-$ $d \to K^+$ $d \to K^-$	1 - $\sqrt{15}$	$0.023 < x < 0.6$ (6 bins)	$0.1 < z < 1.1$ (8 bins)	$W^2 > 10$ GeV^2 $0.1 < y < 0.85$	[46]
COMPASS	1203	$M(x, z, \boldsymbol{P}_{hT}^2, Q)$	$d \to h^+$ $d \to h^-$	1 - 9 (5 bins)	$0.003 < x < 0.4$ (8 bins)	$0.2 < z < 0.8$ (4 bins)	$W^2 > 25$ GeV^2 $0.1 < y < 0.9$	[72]
Total	1547							

MAPTMD 2022

Kinematic coverage

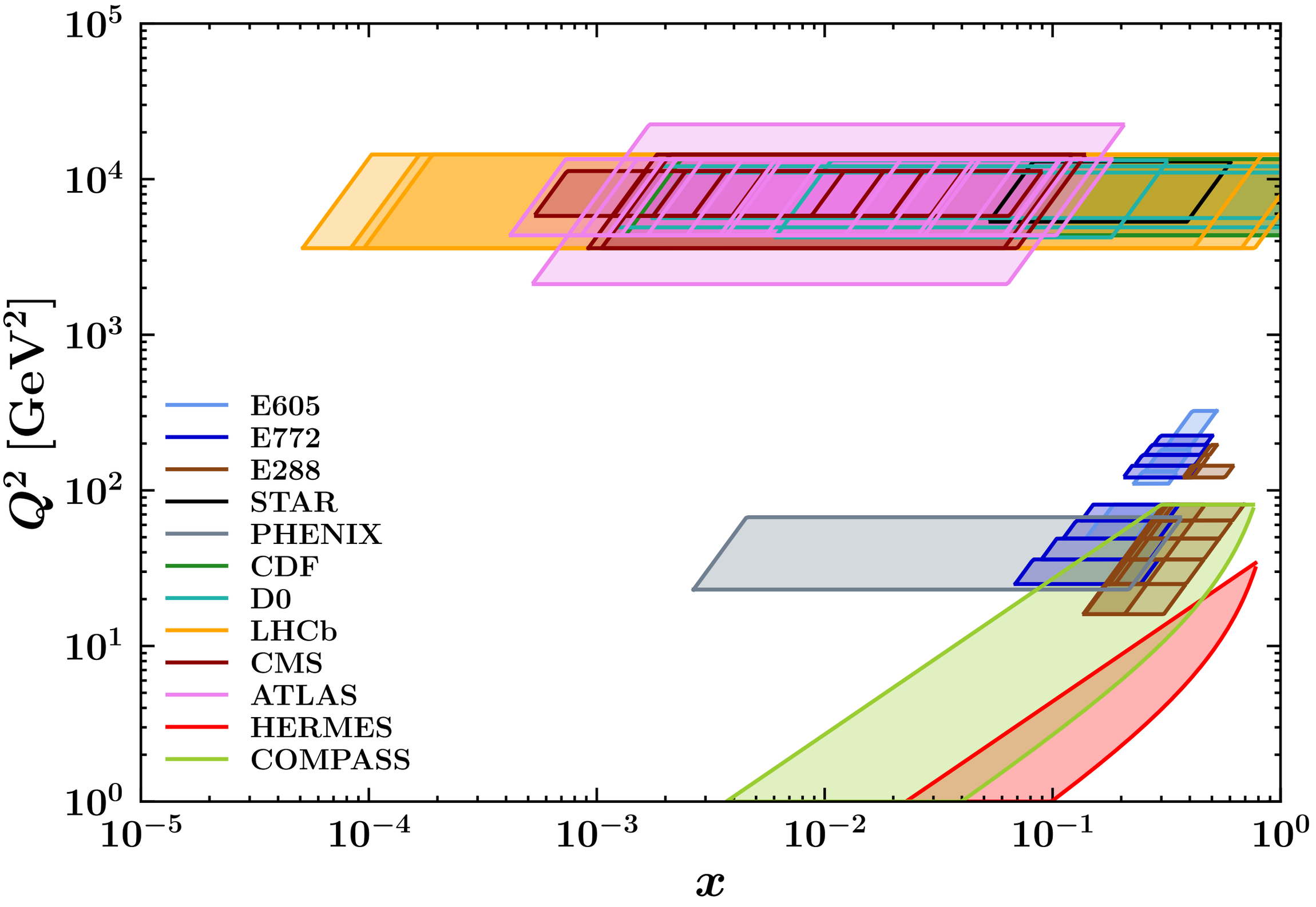

MAPTMD 2022

Fit quality

	N^{3}LL$^-$			
Data set	$N_{\rm dat}$	χ^2_D	χ^2_λ	χ^2_0
CDF Run I	25	0.45	0.09	0.54
CDF Run II	26	0.995	0.004	1.0
D0 Run I	12	0.67	0.01	0.68
D0 Run II	5	0.89	0.21	1.10
D0 Run II (μ)	3	3.96	0.28	4.2
Tevatron total	71	0.87	0.06	0.93
LHCb 7 TeV	7	1.24	0.49	1.73
LHCb 8 TeV	7	0.78	0.36	1.14
LHCb 13 TeV	7	1.42	0.06	1.48
LHCb total	21	1.15	0.3	1.45
ATLAS 7 TeV	18	6.43	0.92	7.35
ATLAS 8 TeV	48	3.7	0.32	4.02
ATLAS 13 TeV	6	5.9	0.5	6.4
ATLAS total	72	4.56	0.48	5.05
CMS 7 TeV	4	2.21	0.10	2.31
CMS 8 TeV	4	1.938	0.001	1.94
CMS 13 TeV	70	0.36	0.02	0.37
CMS total	78	0.53	0.02	0.55
PHENIX 200	2	2.21	0.88	3.08
STAR 510	7	1.05	0.10	1.15
DY collider total	251	1.86	0.2	2.06
E288 200 GeV	30	0.35	0.19	0.54
E288 300 GeV	39	0.33	0.09	0.42
E288 400 GeV	61	0.5	0.11	0.61
E772	53	1.52	1.03	2.56
E605	50	1.26	0.44	1.7
DY fixed-target total	233	0.85	0.4	1.24
HERMES ($p \to \pi^+$)	45	0.86	0.42	1.28
HERMES ($p \to \pi^-$)	45	0.61	0.31	0.92
HERMES ($p \to K^+$)	45	0.49	0.04	0.53
HERMES ($p \to K^-$)	37	0.18	0.13	0.31
HERMES ($d \to \pi^+$)	41	0.68	0.45	1.13
HERMES ($d \to \pi^-$)	45	0.63	0.35	0.97
HERMES ($d \to K^+$)	45	0.2	0.02	0.22
HERMES ($d \to K^-$)	41	0.14	0.08	0.22
HERMES total	344	0.48	0.23	0.71
COMPASS ($d \to h^+$)	602	0.55	0.31	0.86
COMPASS ($d \to h^-$)	601	0.68	0.3	0.98
COMPASS total	1203	0.62	0.3	0.92
SIDIS total	1547	0.59	0.28	0.87
Total	**2031**	**0.77**	**0.29**	**1.06**

MAPTMD 2022

Correlation between fit parameters

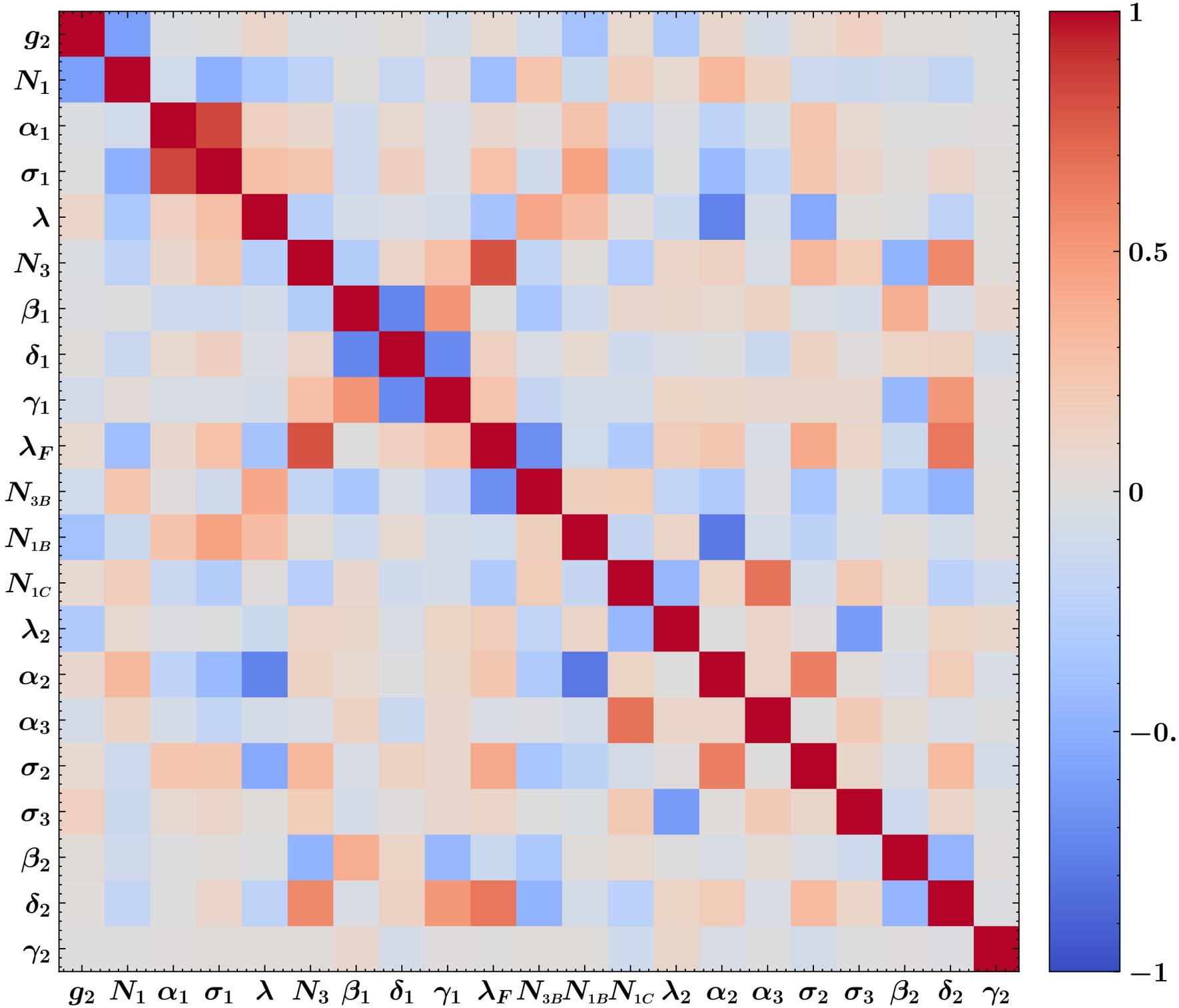

MAPTMD 2022

Collins-Soper kernel

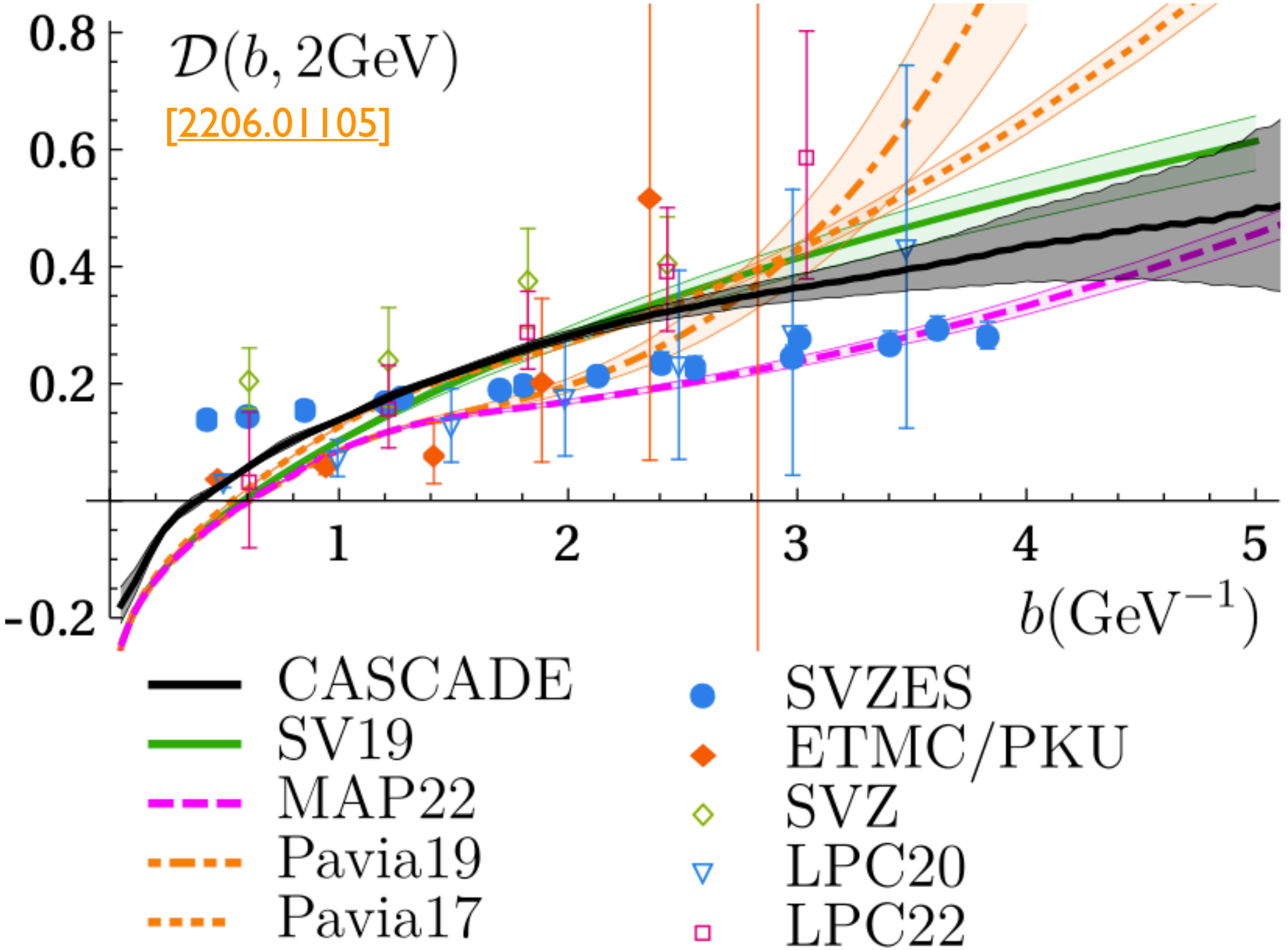

MAPTMD 2022

Fit quality: SIDIS

HERMES

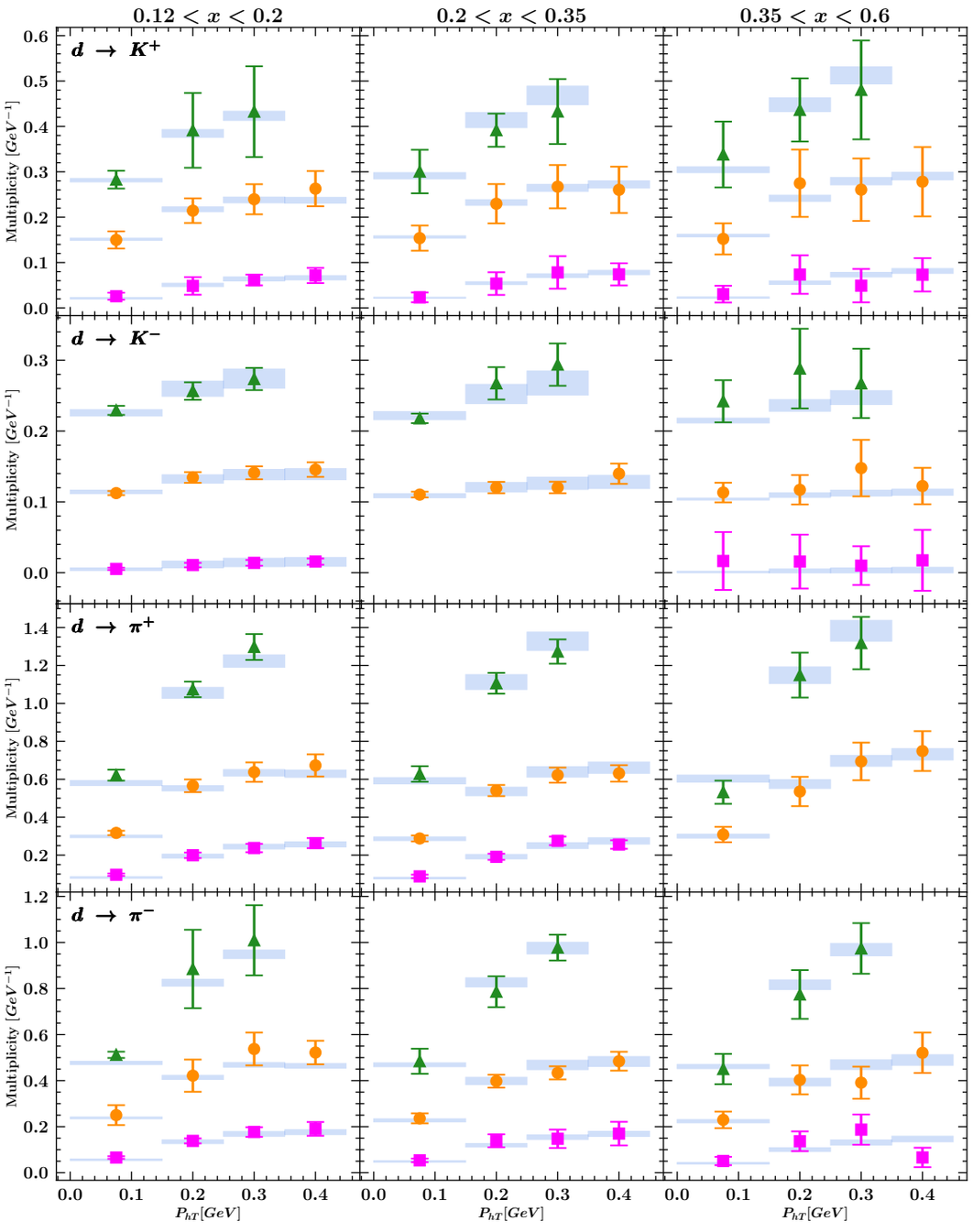

COMPASS h^-

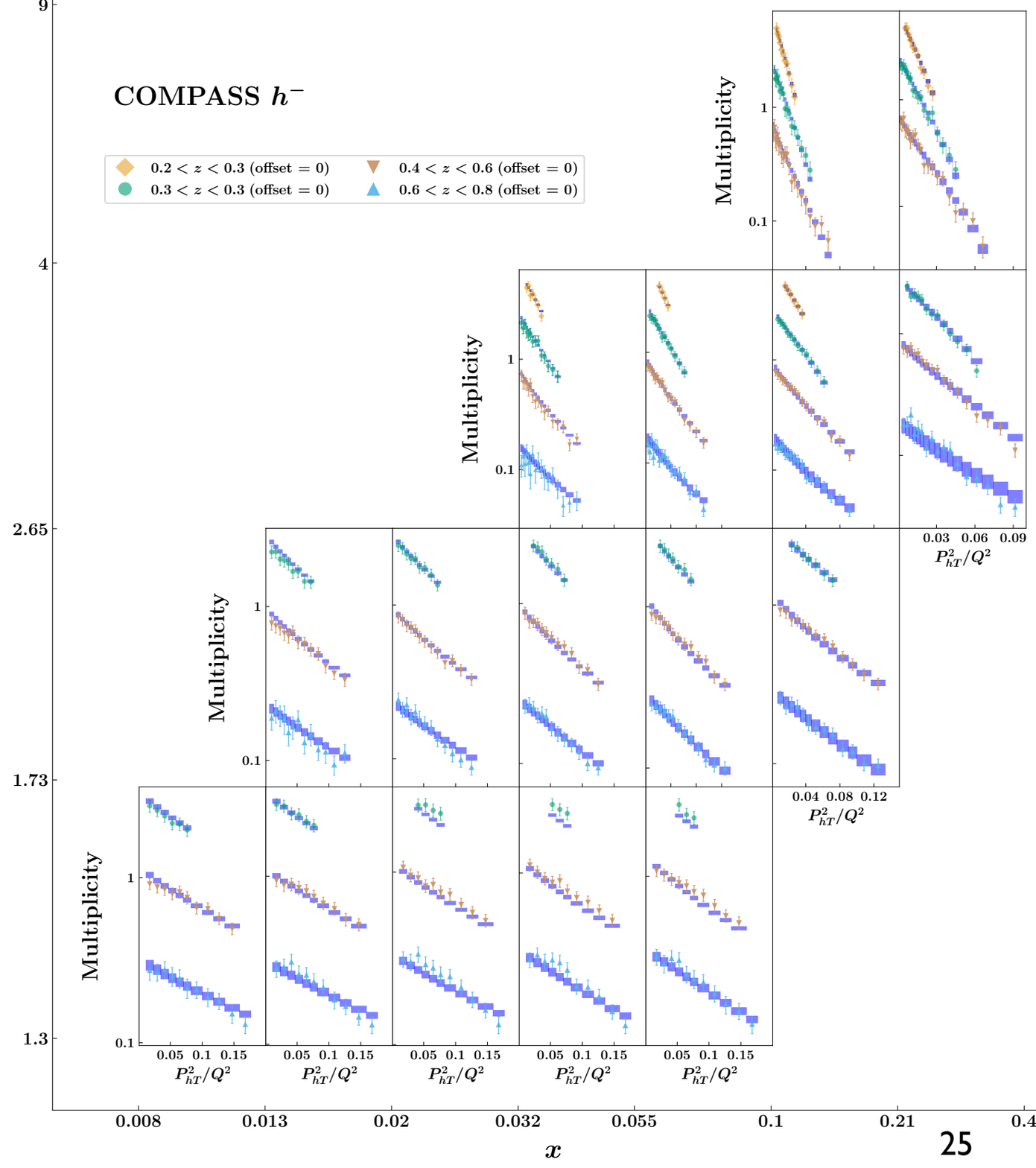

MAPTMD 2022

Fit quality: DY

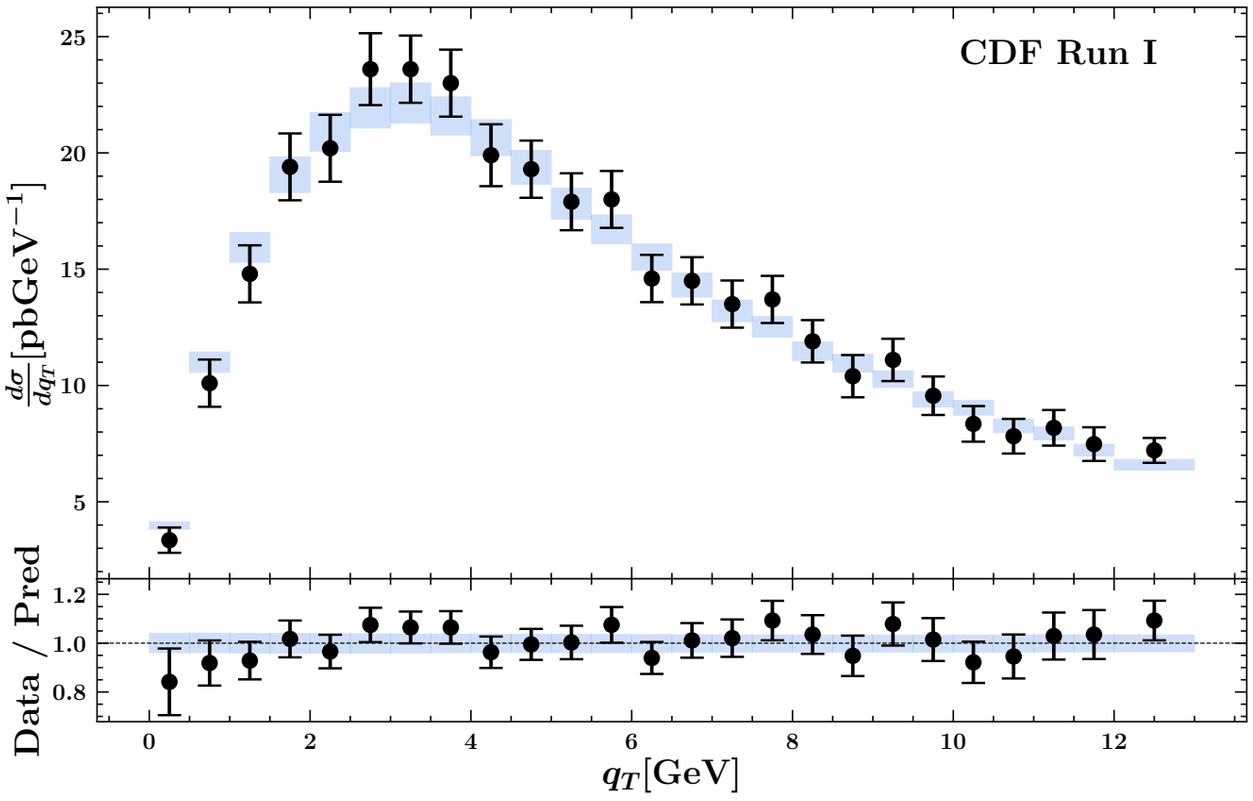

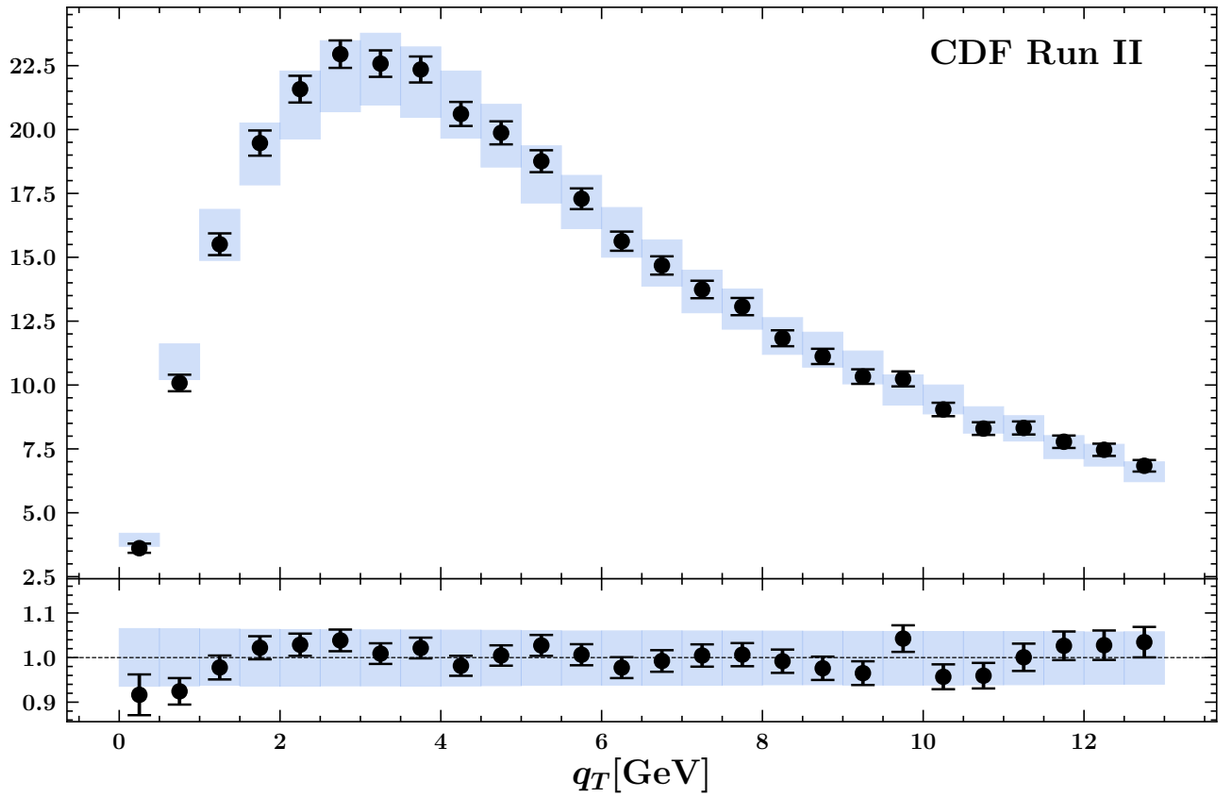

MAPTMD 2022

Fit quality: DY at LHCb

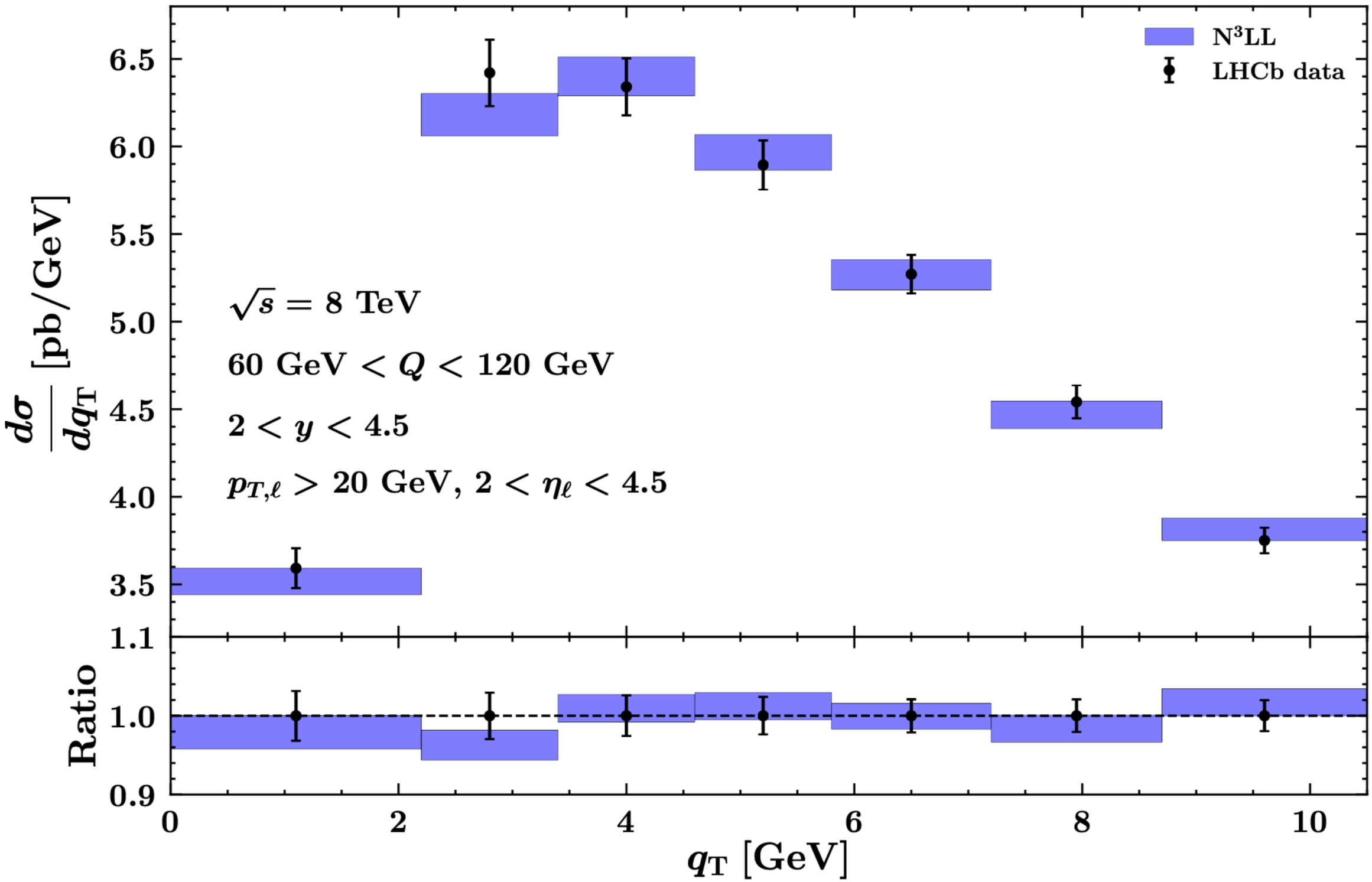

Rapidity-differential data

The role of x-dependence of TMDs

- In [JHEP 07 (2020) 117] (predecessor of MAPTMD22) we studied how the x-dependence of TMDs affects the fit quality.
- To do so, we employed a particularly simple and ***x*-independent** parameterisation for the TMD PDFs:

$$f_{\rm NP}^{\rm DWS}(b_T,\zeta) = \exp\left[-\frac{1}{2}\left(g_1 + g_2 \ln\left(\frac{\zeta}{2Q_0^2}\right)\right) b_T^2\right]$$

- We found that x-dependence is crucial to achieve an accurate description of rapidity differential data (from ATLAS):

	Full dataset	No y-differential data
Global $\chi^2/N_{\rm dat}$	1.339	0.895

- Indeed, in DY: $x_{1,2} = \dfrac{Q}{\sqrt{s}} e^{\pm y}$
- It is particularly important to have **rapidity-dependent data**:
  - **forward data** is important to pin down PDFs at small and large x.

Perturbative convergence

	NLL′	NNLL	NNLL′	N^{3}LL
Global χ^2	1126	571	379	360

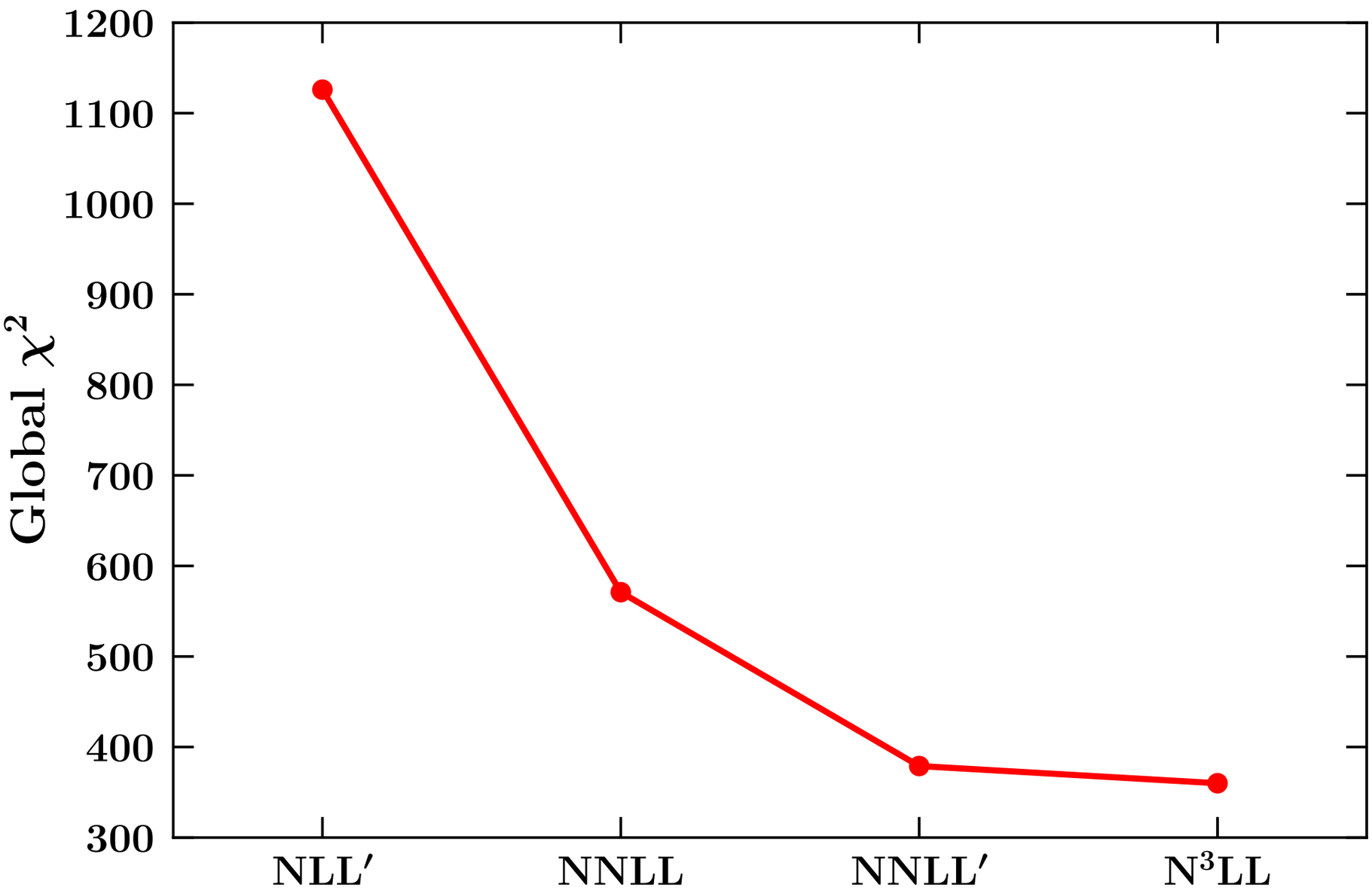

Perturbative convergence

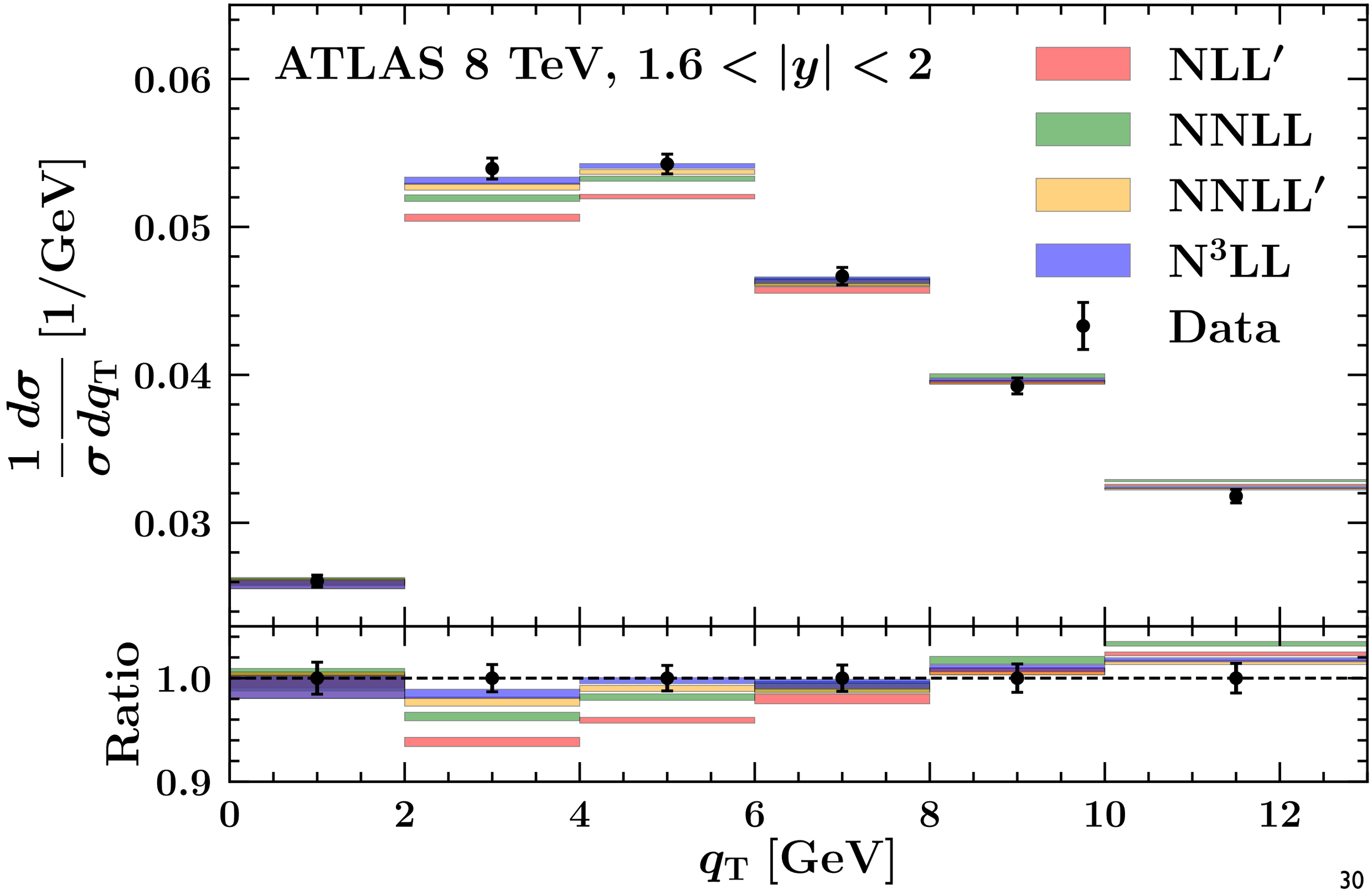

TMDs at the LHC

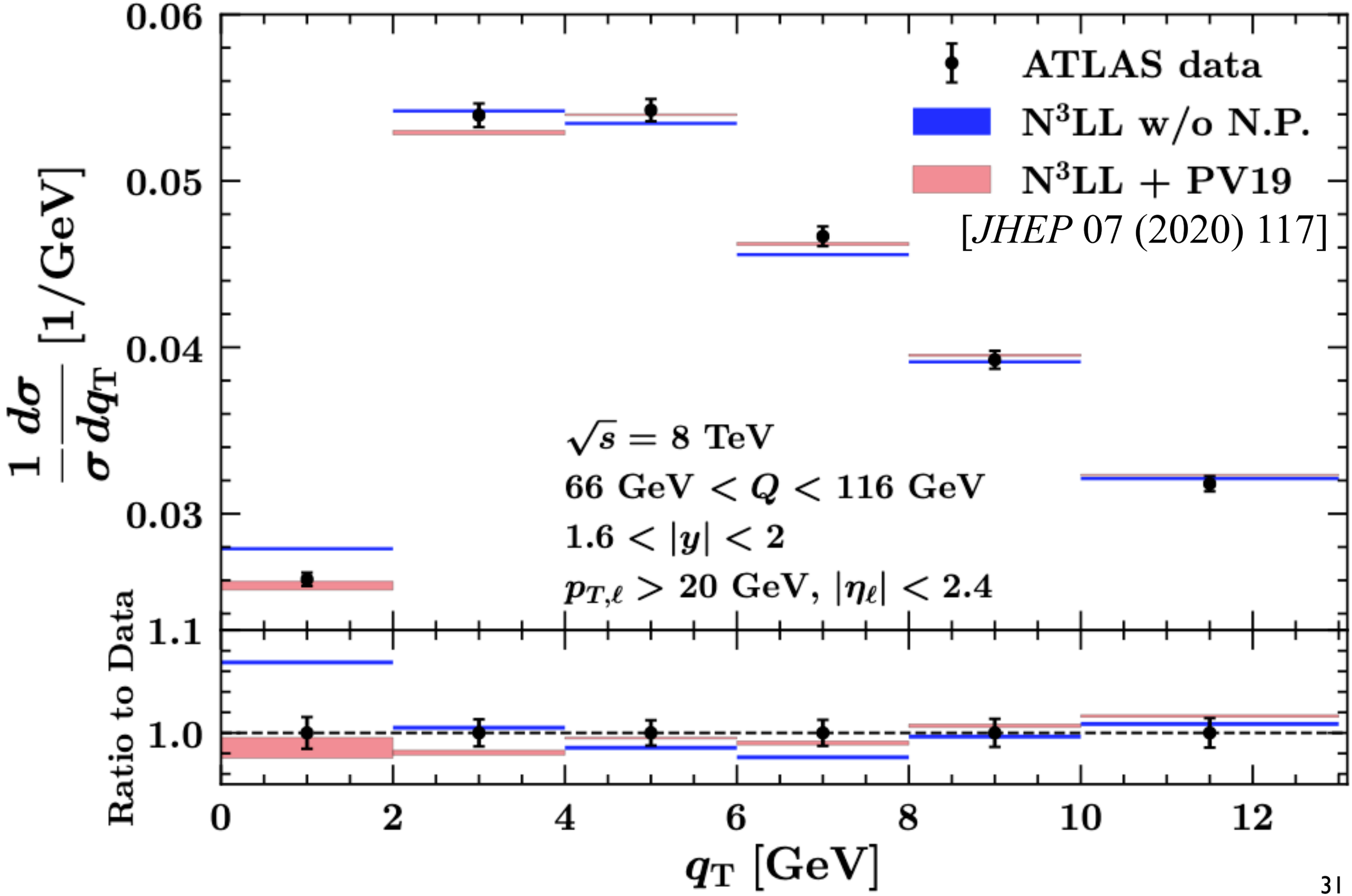

TMDs at the LHC

- Measurements of $Z\,q_T$ distributions have reached **sub-percent level** uncs.:

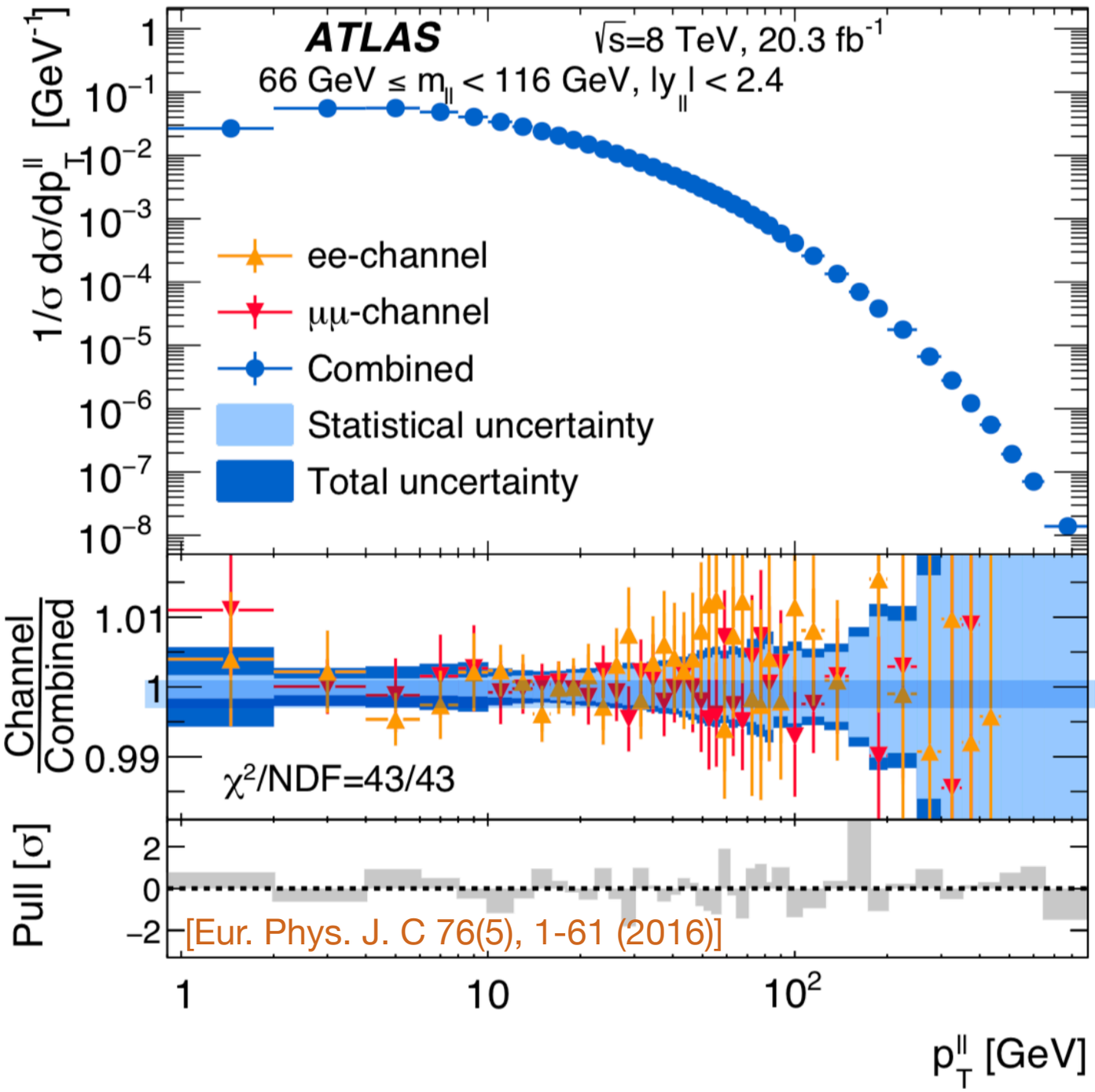

- **State-of-the-art** calculations are thus necessary to describe this data.
- **Non-perturbative** corrections are *very* relevant a very low q_T.

TMDs at the LHC

The W mass

- A precise determination of the ***W* mass** plays an important role in testing the Standard Model and thus for **BSM** physics.

- This is a central task of the **LHC physics programme**.

- In order to minimise experimental systematic effects, the most promising procedure relies on the measurement of the W/Z ratio cross section:

  - the W mass is basically determined through template fits of:

$$\frac{d\sigma^W}{dq_T} = \left(\frac{d\sigma^W/dq_T}{d\sigma^Z/dq_T}\right)_{\mathbf{exp.}} \left(\frac{d\sigma^Z}{dq_T}\right)_{\mathbf{th.}}$$

- Therefore, an accurate and reliable prediction of the ***Z* spectrum** is essential.

- **TMD-based predictions** are currently playing an important role within the LHC electroweak working group along **other formalisms**.

Conclusions

- **TMD factorisation** provides a valuable tool to describe q_T distributions at small values of q_T (resummation of large logs),
  - written in terms of **TMD distributions,**
- Non-perturbative component of TMDs is to be determined from **data**.
- A lot of effort is being invested on the extraction of TMD PDFs and FFs:
  - tremendous progress made over the past few years,
  - wide and precise **datasets** (COMPASS, HERMES, LHC and Tevatron exps.),
  - more data to come from the LHC,
  - state-of-the-art **theoretical computation** moving to even higher accuracy,
  - looking forward to the **EIC** to pin down TMDs to unprecedented accuracy.

Backup

TMDs at the EIC

- An important step is the definition of the relevant **observables** to be measure and the respective **binning**.

- TMDs are crucial to take this step.

- Binning in x and Q^2 under discussion:

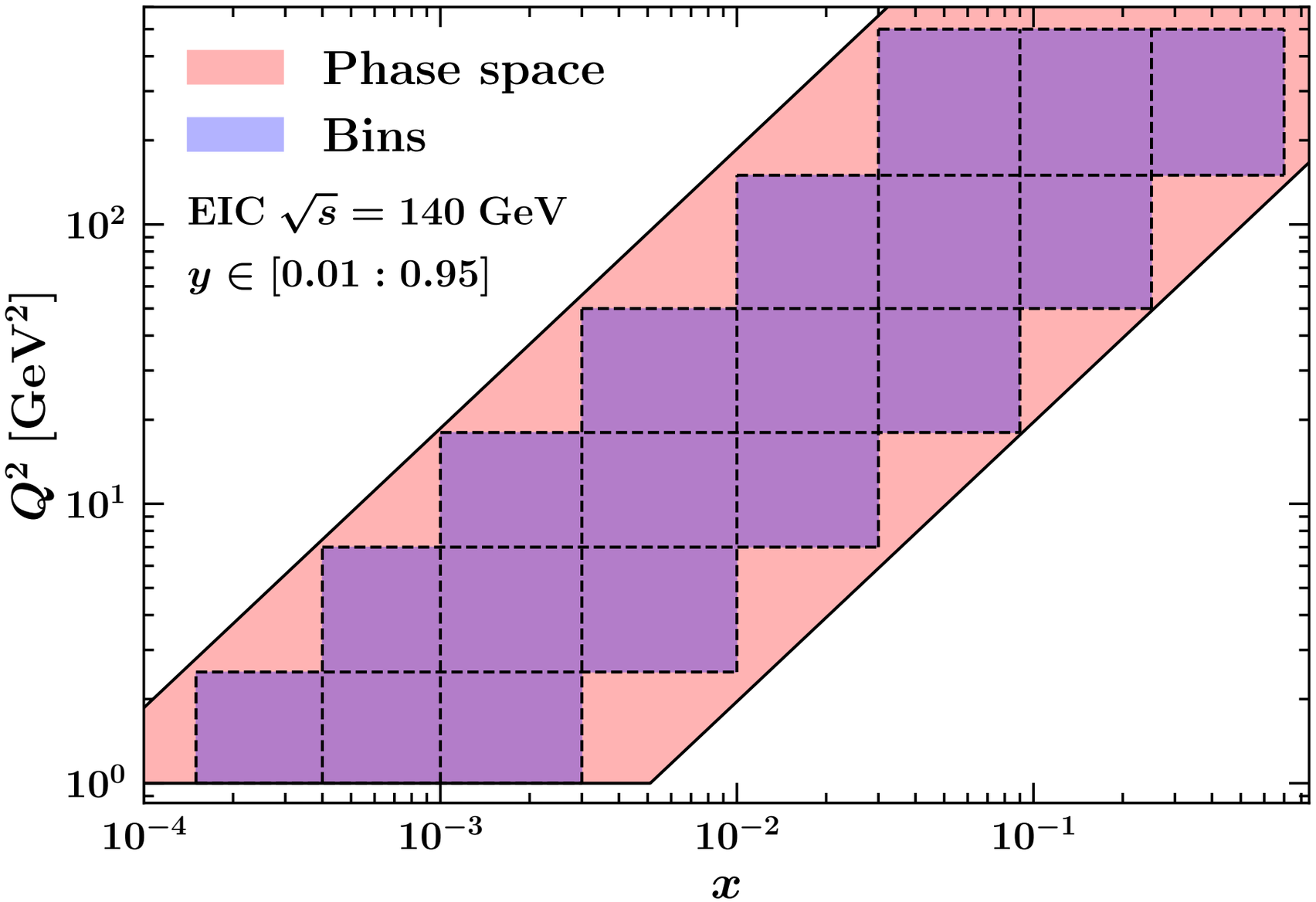

TMDs at the EIC

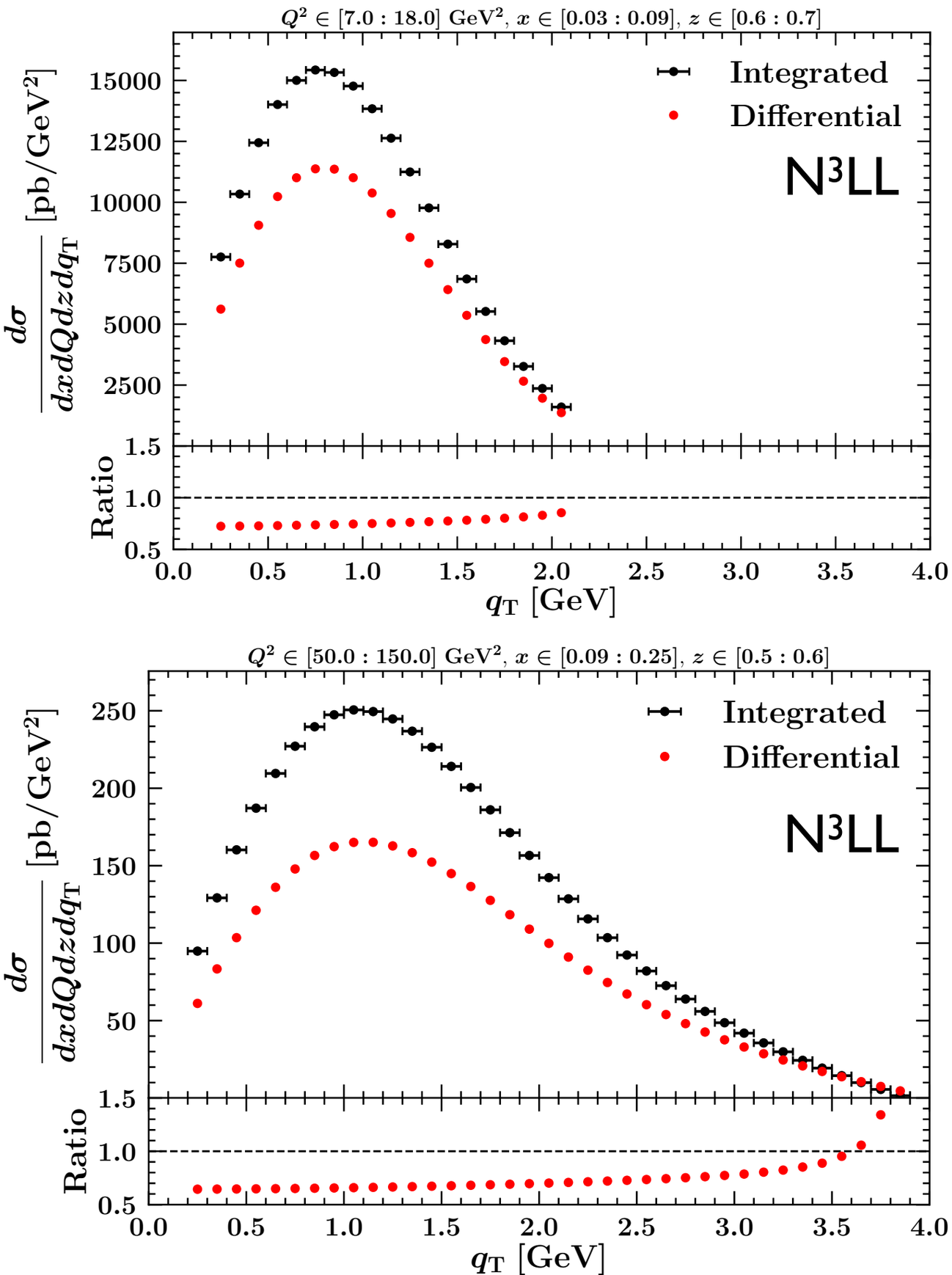

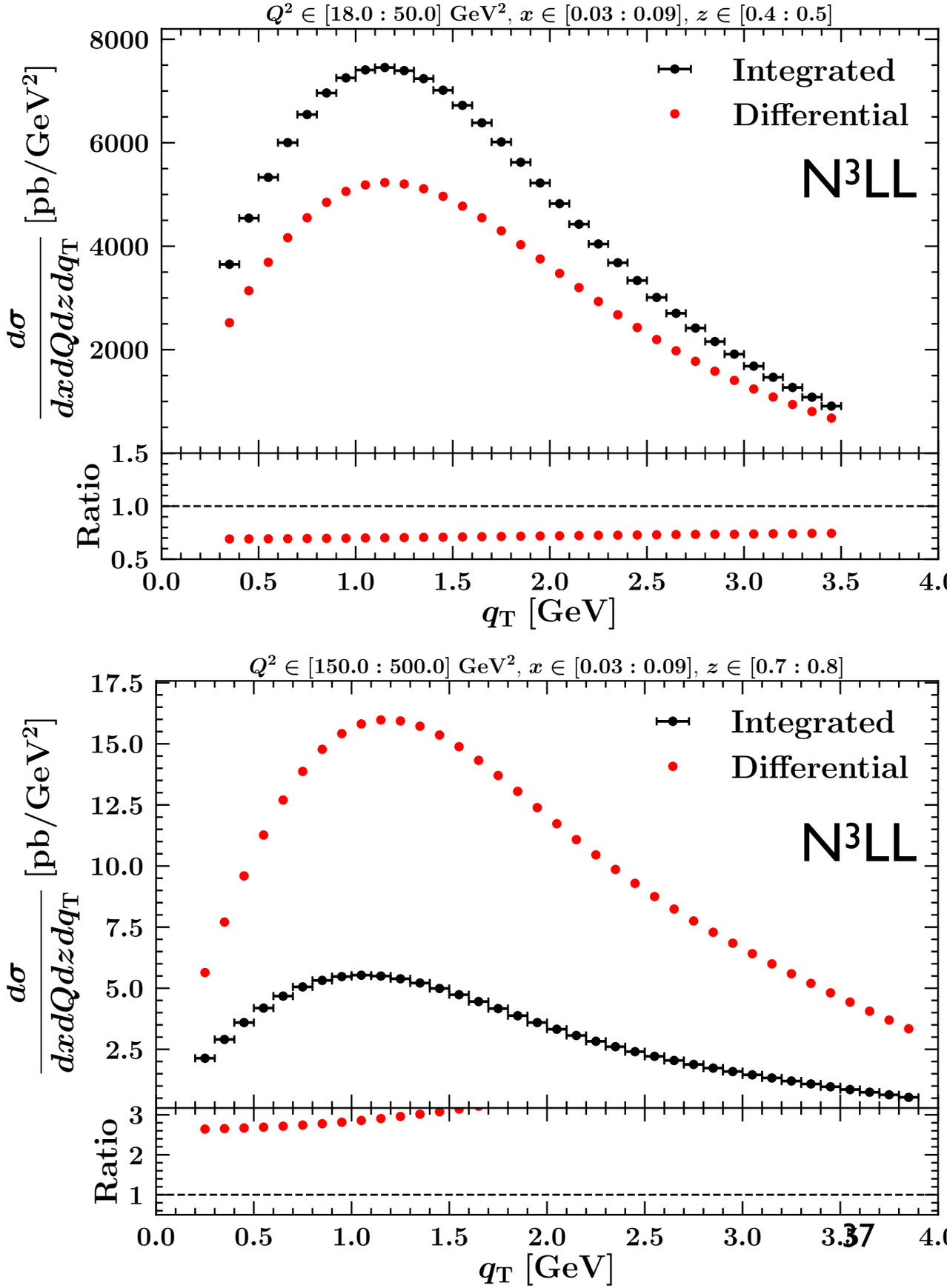

Gluon TMDs

- The *linearly polarised* (h_{T}) and *unpolarised* (f) gluon TMD PDFs contribute to the low-q_{T} spectrum of Higgs production in gluon fusion:

$$\frac{d\sigma}{dyd^2\boldsymbol{q}_T} = \frac{\sigma_{gg\to H}}{(2\pi)^2}\int d^2\boldsymbol{b}\, e^{-i(\boldsymbol{b}\boldsymbol{q}_T)}\left(f_{1,g}(x_A,\boldsymbol{b})f_{1,g}(x_B,\boldsymbol{b}) + h_{1,g}^{\perp}(x_A,\boldsymbol{b})h_{1,g}^{\perp}(x_B,\boldsymbol{b})\right)$$

- Despite linearly polarised gluons enter at NNLL, their effect on the cross section can be assessed but **below current LHC data accuracy**:

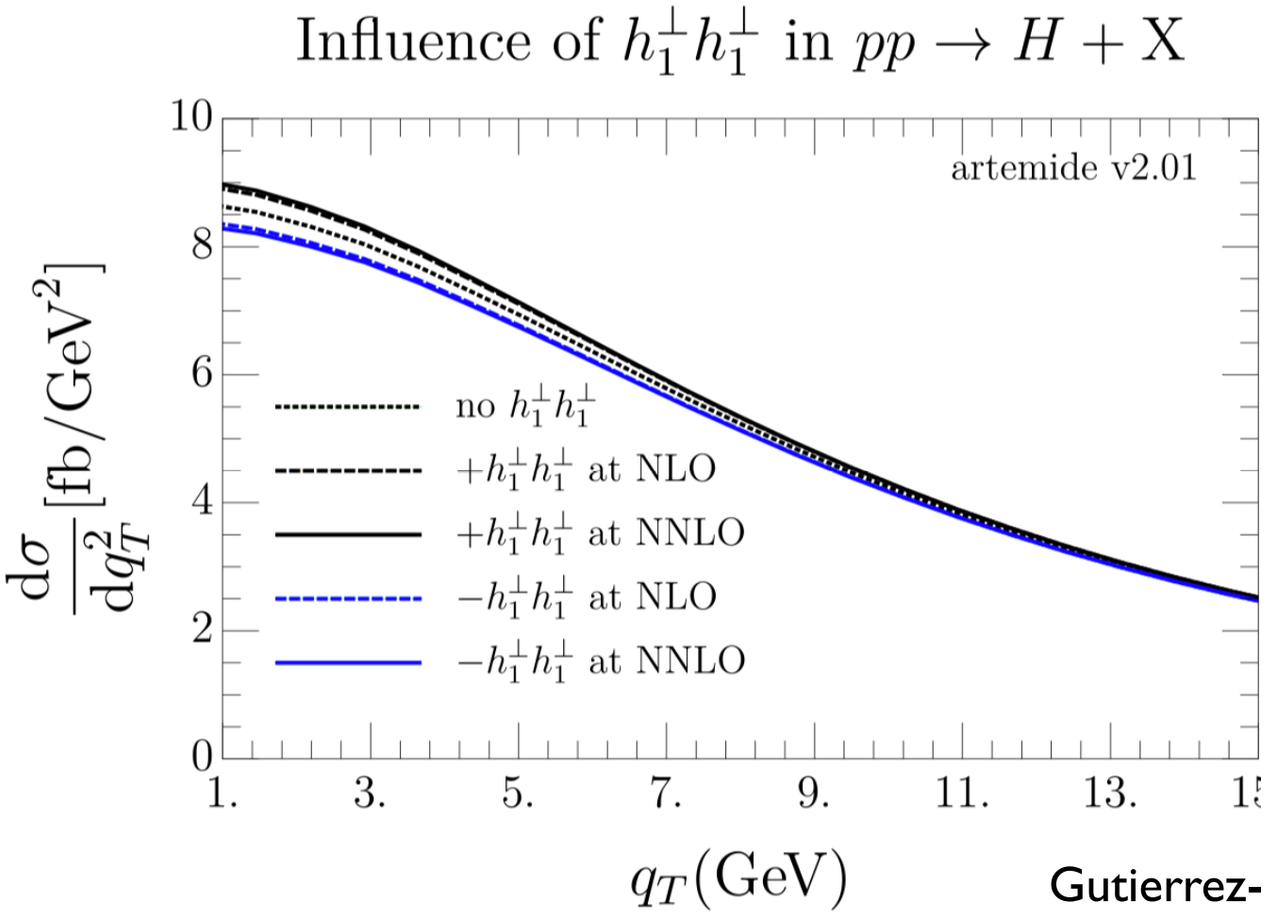

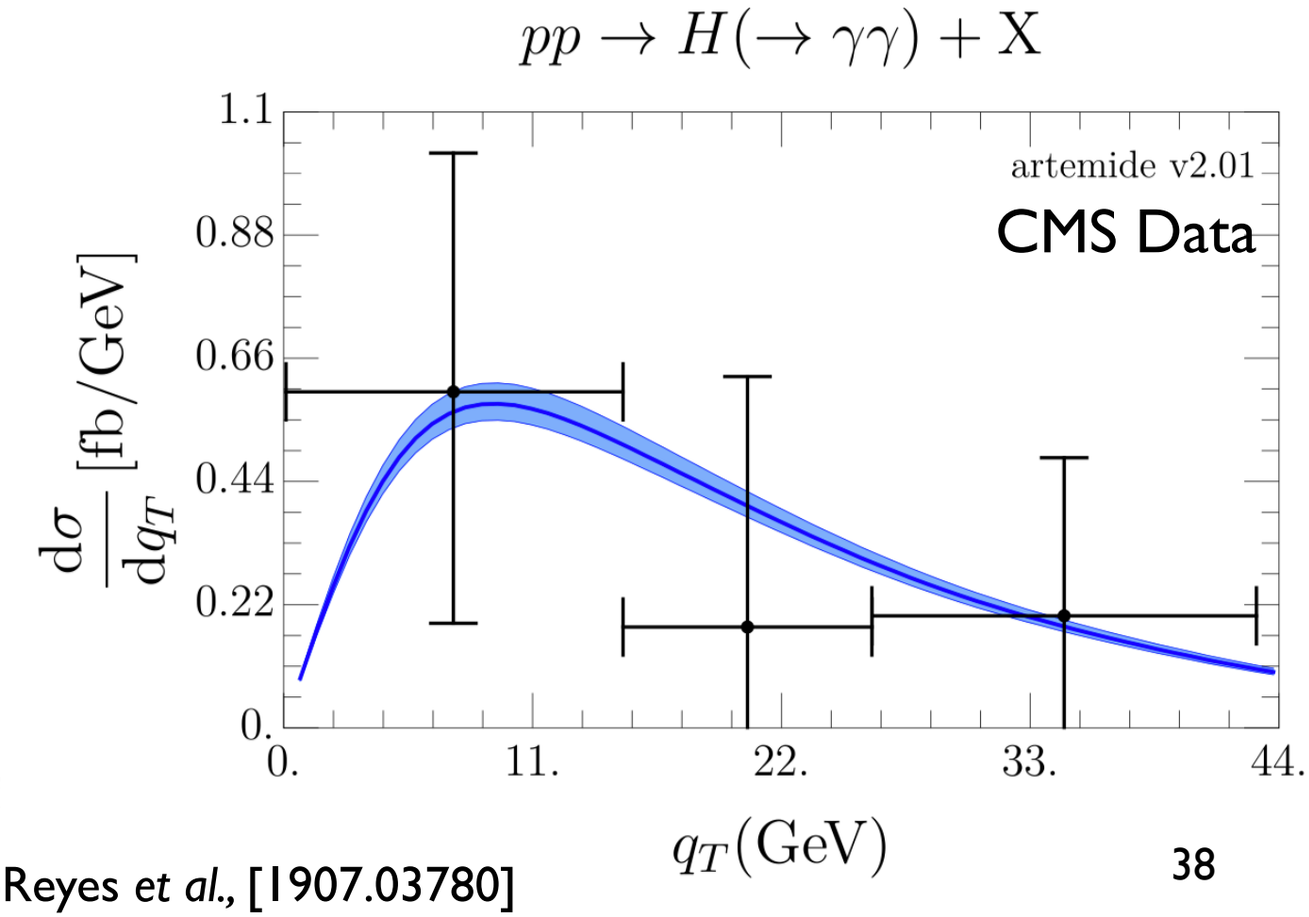

Gutierrez-Reyes *et al.*, [1907.03780]

Logarithmic counting

- TMD factorisation provides **resummation** of large logs $L = \log(q_T/Q)$:
  - implemented through the **Sudakov** form fact R.
- A **perturbative expansion** in powers of α_s of R would give:

One Sudakov for each TMD → $R^2 = \sum_{n=0}^{\infty} a_s^n \sum_{k=1}^{2n} \widetilde{S}^{(n,k)} L^k$ ← Double-log expansion

- that can be rearranged as:

$$R^2 = \sum_{m=0}^{\infty} R^2_{\mathrm{N^mLL}} \quad \text{with} \quad R^2_{\mathrm{N^mLL}} = \sum_{n=[m/2]}^{\infty} \widetilde{S}^{(n,2n-m)}\, a_s^n L^{2n-m}$$

$n=[m/2]$ Integer part of m/2

- Therefore, multiplying R by a power p of α_s gives:

$$a_s^p R^2_{\mathrm{N^mLL}} = \sum_{j=[(m+2p)/2]}^{\infty} \widetilde{S}^{(j-p,2j-(m+2p))}\, a_s^j L^{2j-(m+2p)} \sim R^2_{\mathrm{N^{m+2p}LL}}$$

- Bottom line: any additional power of α_s causes a shift of **two units** in the logarithmic ordering.

MAPTMD 2022

Normalisation of SIDIS

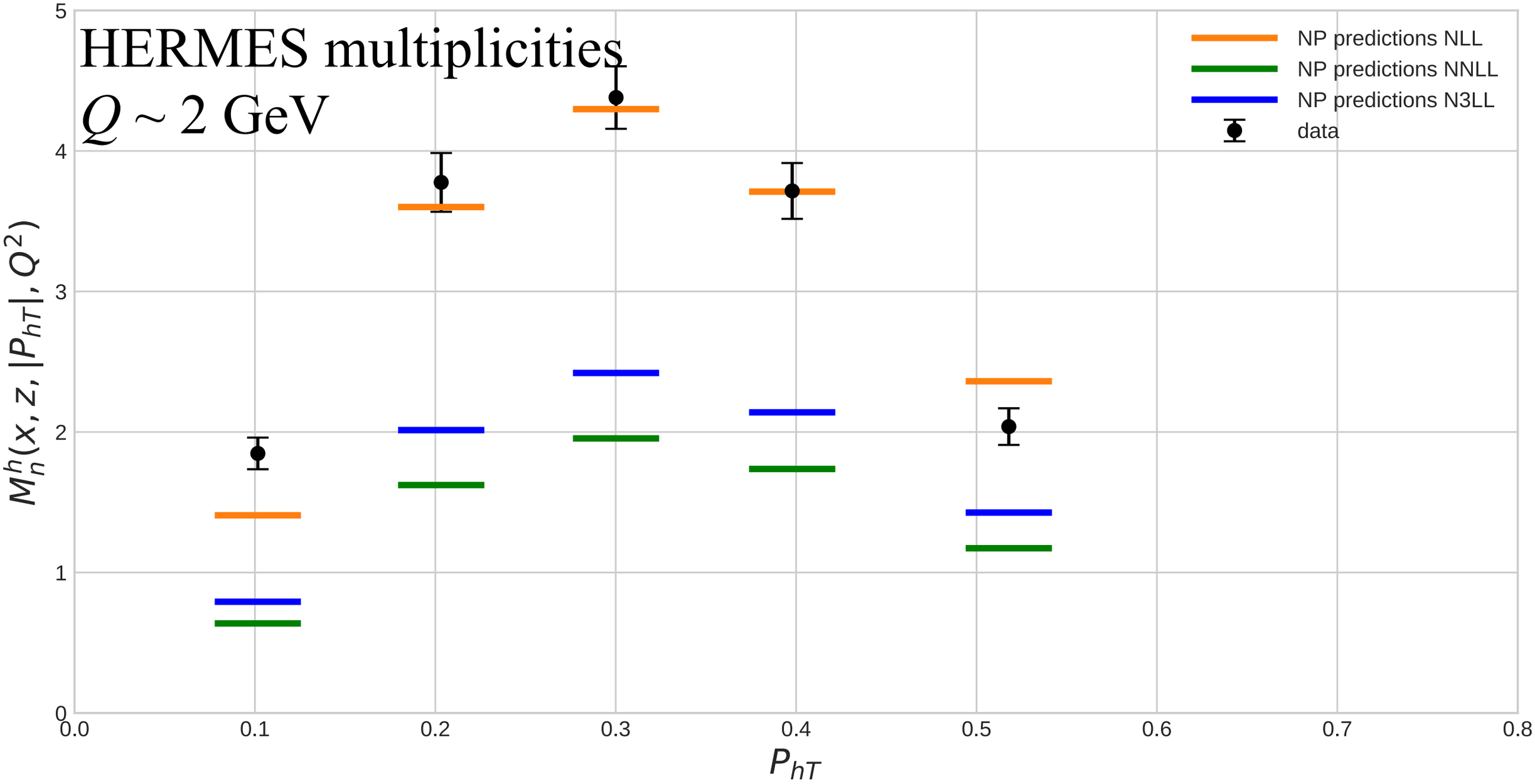

- Description of SIDIS multiplicities considerably worsens moving from NLL to higher perturbative orders.

MAPTMD 2022

Normalisation of SIDIS

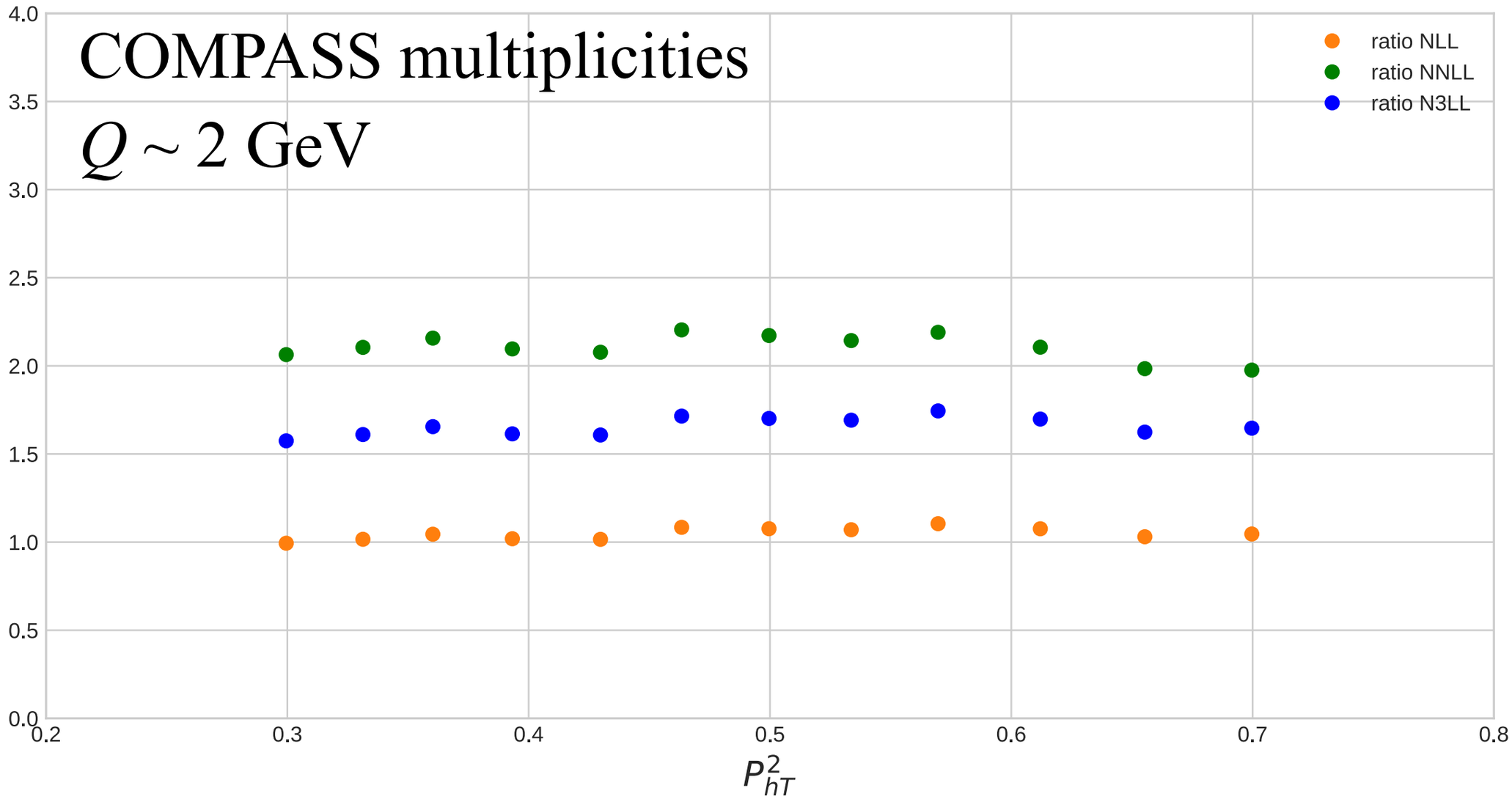

- Normalisation problem already observed in the literature.
- Large perturbative corrections particularly to the hard function:

$$H_{\text{SIDIS}}(Q) = 1 + \frac{\alpha_s(Q)}{4\pi} \underbrace{C_F \left(-16 + \frac{\pi^2}{3}\right)}_{\sim -17} + \mathcal{O}(\alpha_s^2)$$

MAPTMD 2022

Normalisation of SIDIS

- SIDIS multiplicity: $M(x, z, P_{hT}, Q) = \dfrac{d\sigma}{dx dQ dz dP_{hT}} \Big/ \dfrac{d\sigma}{dx dQ}$
- The SIDIS cross section integrated over P_{hT} ($d\sigma/dx dQ dz$) is ok.

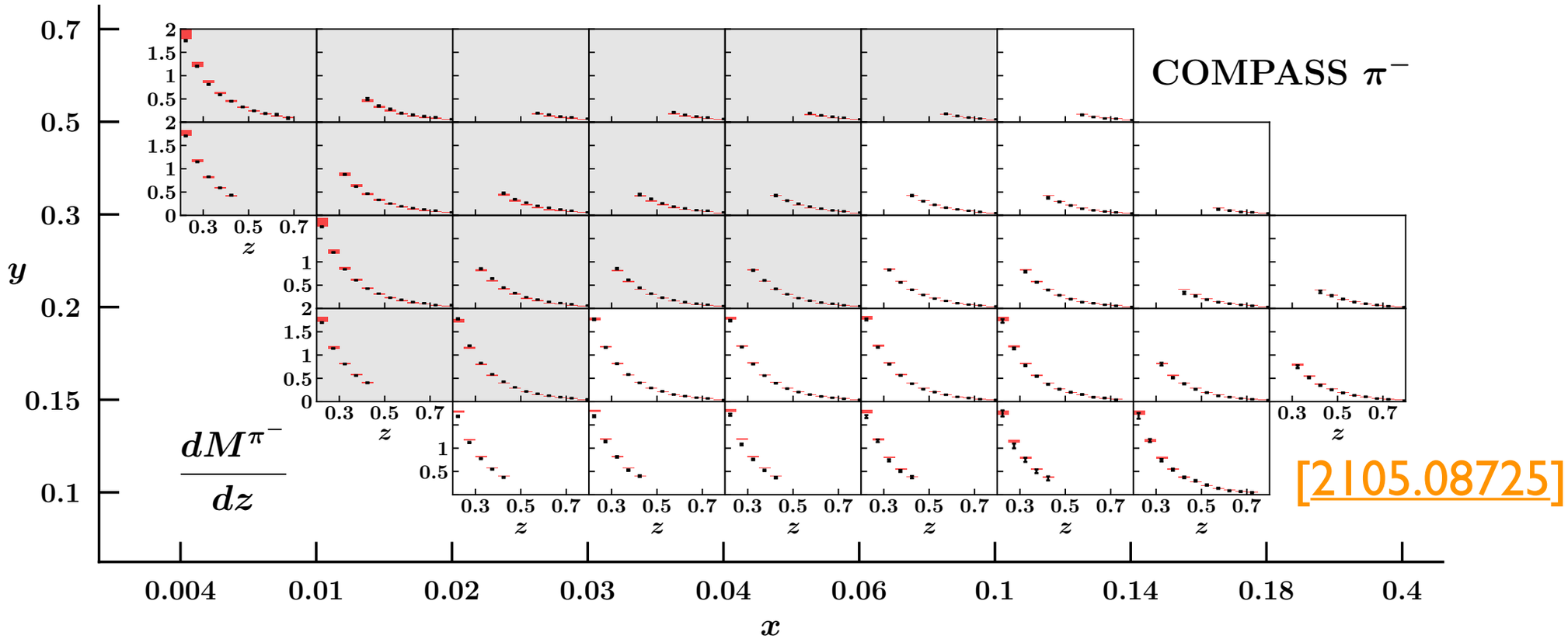

[2105.08725]

- Normalise predictions such that integral over P_{hT} gives $d\sigma/dx dQ dz$:

$$M(x, z, P_{hT}, Q) = \mathcal{N} \frac{\dfrac{d\sigma}{dx dQ dz dP_{hT}}}{\dfrac{d\sigma}{dx dQ}} \qquad \mathcal{N} = \frac{\dfrac{d\sigma}{dx dQ dz}}{\displaystyle\int dP_{hT} \frac{d\sigma}{dx dQ dz dP_{hT}}}$$

- Theoretically determined normalisation, **not fitted**.

MAPTMD 2022

Normalisation of SIDIS

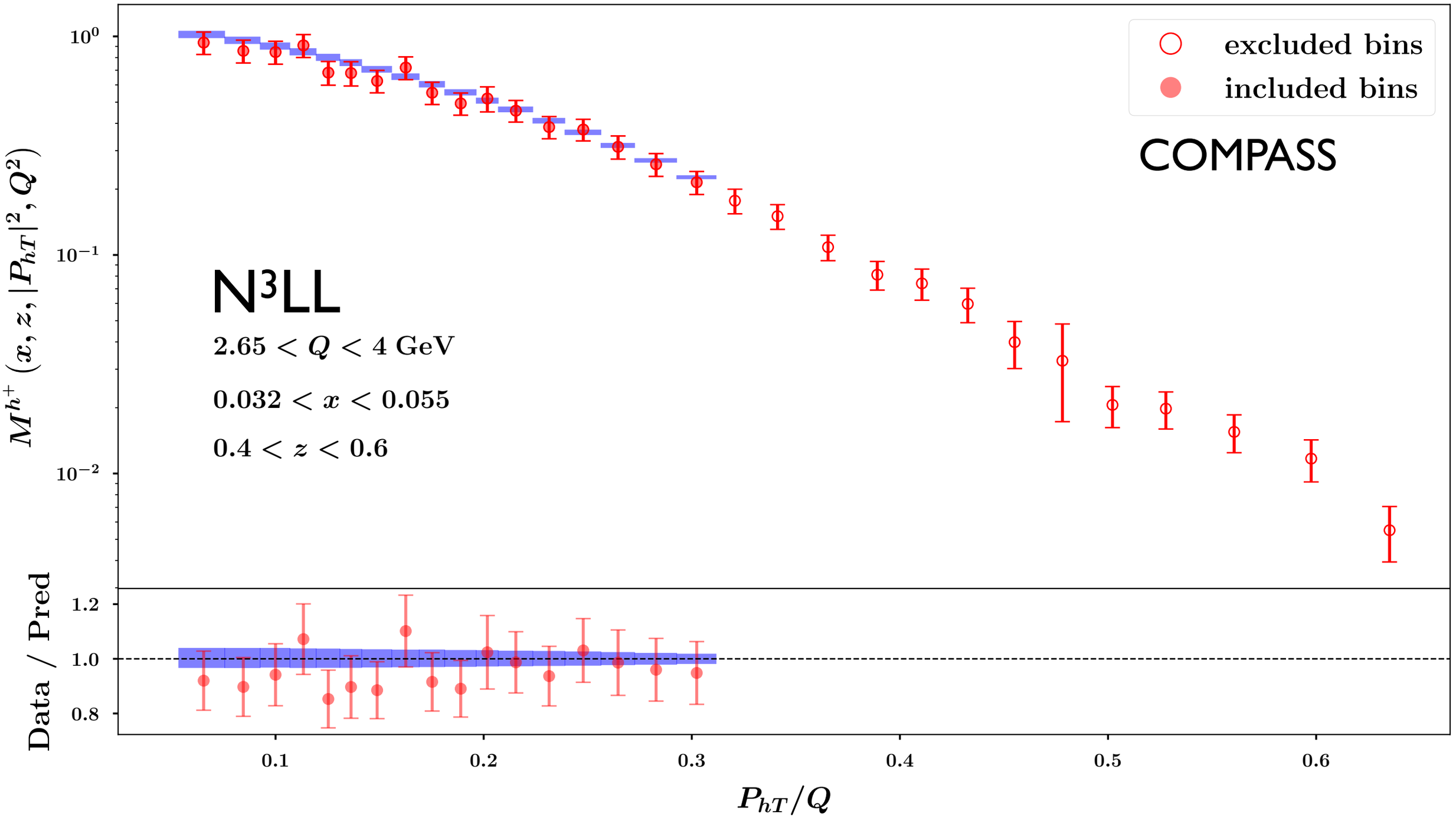

- Excellent agreement upon normalisation.

MAPTMD 2022

Normalisation of SIDIS

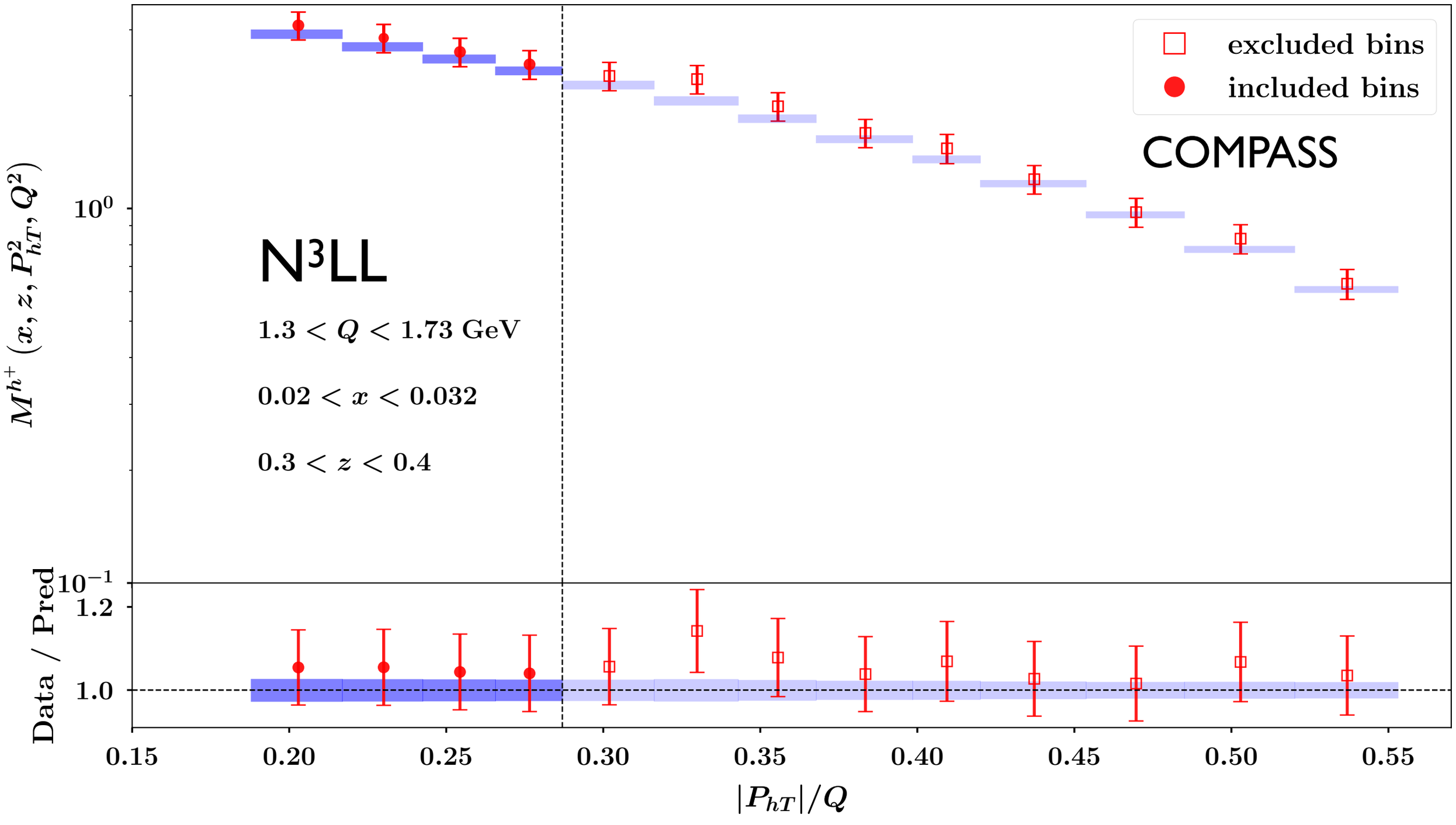

- Agreement extends well above the expected validity region. To be clarified.

Pavia2019

Dataset

- DY data only:
  - fixed-target low-energy DY,
  - STAR data
  - LHC and Tevatron data,
  - 353 data points,
  - selection cut q_T / Q < 0.2.

Experiment	N_{dat}	Observable	$\sqrt{s}$ [GeV]	Q [GeV]	y or x_F	Lepton cuts	Ref.
E605	50	$Ed^3\sigma/d^3q$	38.8	7 - 18	$x_F = 0.1$	-	[79]
E288 200 GeV	30	$Ed^3\sigma/d^3q$	19.4	4 - 9	$y = 0.40$	-	[80]
E288 300 GeV	39	$Ed^3\sigma/d^3q$	23.8	4 - 12	$y = 0.21$	-	[80]
E288 400 GeV	61	$Ed^3\sigma/d^3q$	27.4	5 - 14	$y = 0.03$	-	[80]
STAR 510	7	$d\sigma/dq_T$	510	73 - 114	$\lvert y\rvert < 1$	$p_{T\ell} > 25$ GeV $\lvert\eta_\ell\rvert < 1$	-
CDF Run I	25	$d\sigma/dq_T$	1800	66 - 116	Inclusive	-	[81]
CDF Run II	26	$d\sigma/dq_T$	1960	66 - 116	Inclusive	-	[82]
D0 Run I	12	$d\sigma/dq_T$	1800	75 - 105	Inclusive	-	[83]
D0 Run II	5	$(1/\sigma)d\sigma/dq_T$	1960	70 - 110	Inclusive	-	[84]
D0 Run II (μ)	3	$(1/\sigma)d\sigma/dq_T$	1960	65 - 115	$\lvert y\rvert < 1.7$	$p_{T\ell} > 15$ GeV $\lvert\eta_\ell\rvert < 1.7$	[85]
LHCb 7 TeV	7	$d\sigma/dq_T$	7000	60 - 120	$2 < y < 4.5$	$p_{T\ell} > 20$ GeV $2 < \eta_\ell < 4.5$	[86]
LHCb 8 TeV	7	$d\sigma/dq_T$	8000	60 - 120	$2 < y < 4.5$	$p_{T\ell} > 20$ GeV $2 < \eta_\ell < 4.5$	[87]
LHCb 13 TeV	7	$d\sigma/dq_T$	13000	60 - 120	$2 < y < 4.5$	$p_{T\ell} > 20$ GeV $2 < \eta_\ell < 4.5$	[92]
CMS 7 TeV	4	$(1/\sigma)d\sigma/dq_T$	7000	60 - 120	$\lvert y\rvert < 2.1$	$p_{T\ell} > 20$ GeV $\lvert\eta_\ell\rvert < 2.1$	[88]
CMS 8 TeV	4	$(1/\sigma)d\sigma/dq_T$	8000	60 - 120	$\lvert y\rvert < 2.1$	$p_{T\ell} > 15$ GeV $\lvert\eta_\ell\rvert < 2.1$	[89]
ATLAS 7 TeV	6 6 6	$(1/\sigma)d\sigma/dq_T$	7000	66 - 116	$\lvert y\rvert < 1$ $1 < \lvert y\rvert < 2$ $2 < \lvert y\rvert < 2.4$	$p_{T\ell} > 20$ GeV $\lvert\eta_\ell\rvert < 2.4$	[93]
ATLAS 8 TeV on-peak	6 6 6 6 6 6	$(1/\sigma)d\sigma/dq_T$	8000	66 - 116	$\lvert y\rvert < 0.4$ $0.4 < \lvert y\rvert < 0.8$ $0.8 < \lvert y\rvert < 1.2$ $1.2 < \lvert y\rvert < 1.6$ $1.6 < \lvert y\rvert < 2$ $2 < \lvert y\rvert < 2.4$	$p_{T\ell} > 20$ GeV $\lvert\eta_\ell\rvert < 2.4$	[90]
ATLAS 8 TeV off-peak	4 8	$(1/\sigma)d\sigma/dq_T$	8000	46 - 66 116 - 150	$\lvert y\rvert < 2.4$	$p_{T\ell} > 20$ GeV $\lvert\eta_\ell\rvert < 2.4$	[90]
Total	353	-	-	-	-	-	-

Pavia2019

Kinematic coverage

$$x_{1,2} = \frac{Q}{\sqrt{s}} e^{\pm y}$$

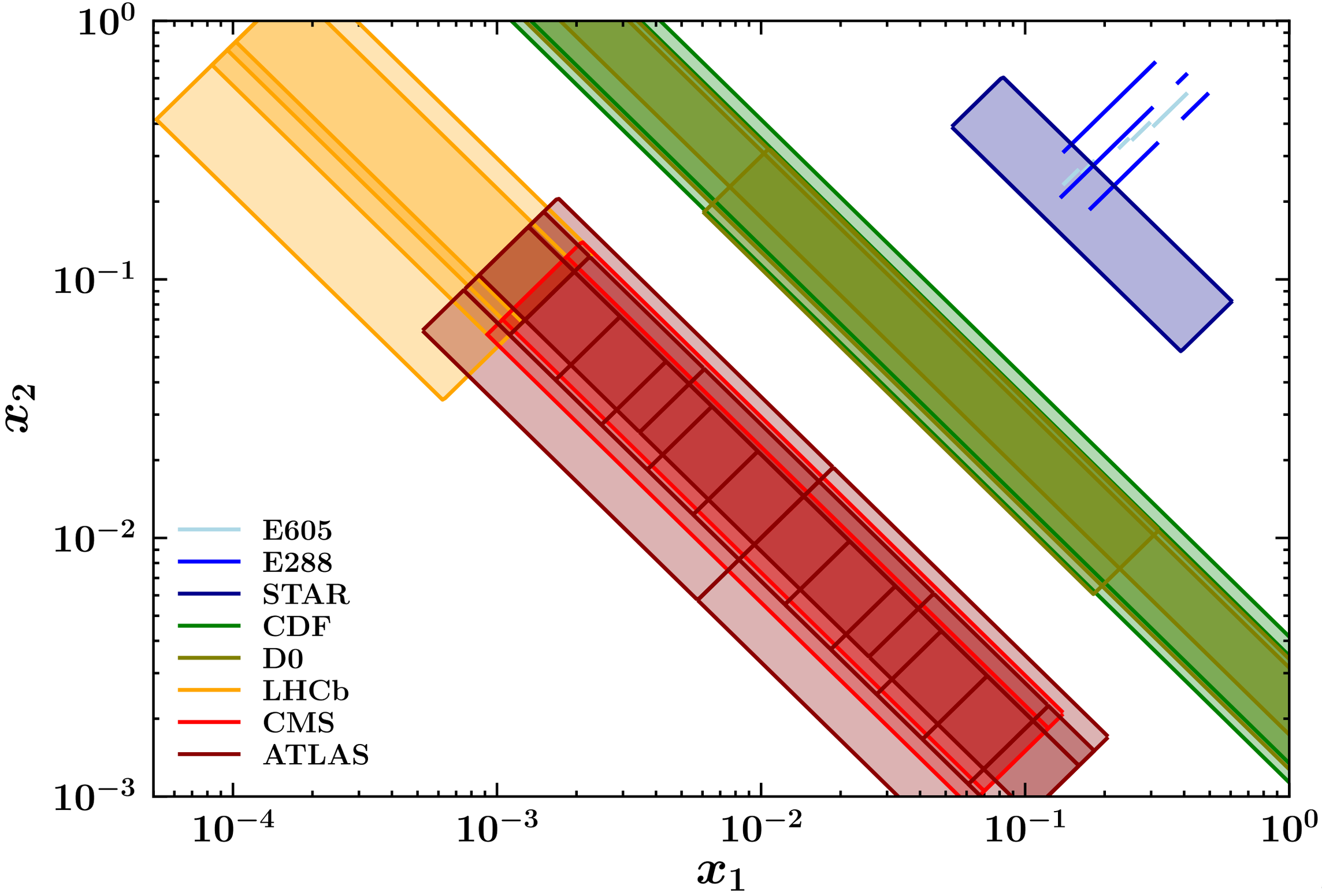

Pavia2019

Main settings

- b_* prescription:

$$b_*(b_T) = b_{\max}\left(\frac{1-e^{-b_T^4/b_{\max}^4}}{1-e^{-b_T^4/b_{\min}^4}}\right)^{1/4} \quad \text{with} \quad \begin{cases} b_{\max} = 2e^{-\gamma_E} \\ b_{\min} = b_{\max}/Q \end{cases}$$

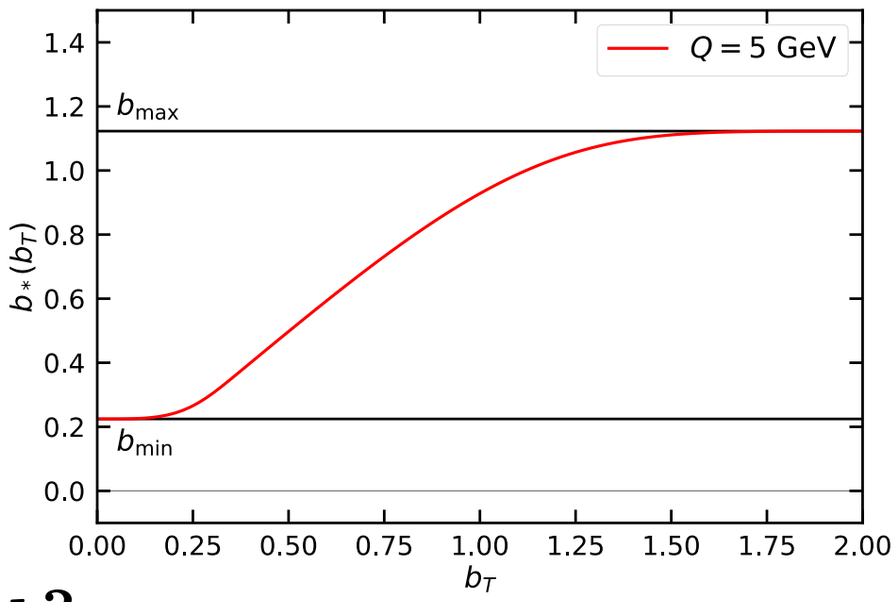

- Non-perturbative function $f_{\rm NP}$:
  - evolution:

$$\boldsymbol{g_K(b_T) = -\left(g_2 + g_{2B}b_T^2\right)\frac{b_T^2}{2}}$$

  - PDFs:

$$\widetilde{f}_{\rm NP}(x, b_T) = \left[\frac{1-\lambda}{1+g_1(x)\frac{b_T^2}{4}} + \lambda \exp\left(-g_{1B}(x)\frac{b_T^2}{4}\right)\right]$$

$$g_1(x) = \frac{N_1}{x\sigma}\exp\left[-\frac{1}{2\sigma^2}\ln^2\left(\frac{x}{\alpha}\right)\right] \qquad g_{1B}(x) = \frac{N_{1B}}{x\sigma_B}\exp\left[-\frac{1}{2\sigma_B^2}\ln^2\left(\frac{x}{\alpha_B}\right)\right]$$

- **9 free parameters** to fit to data.
- Perturbative accuracies: **NLL', NNLL, NNLL', N³LL**
- **Monte Carlo** method for the experimental error propagation.

Pavia2019

Fit quality

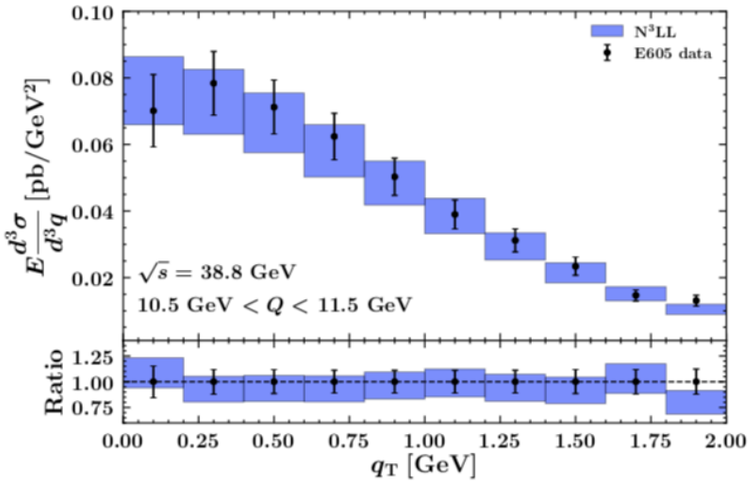

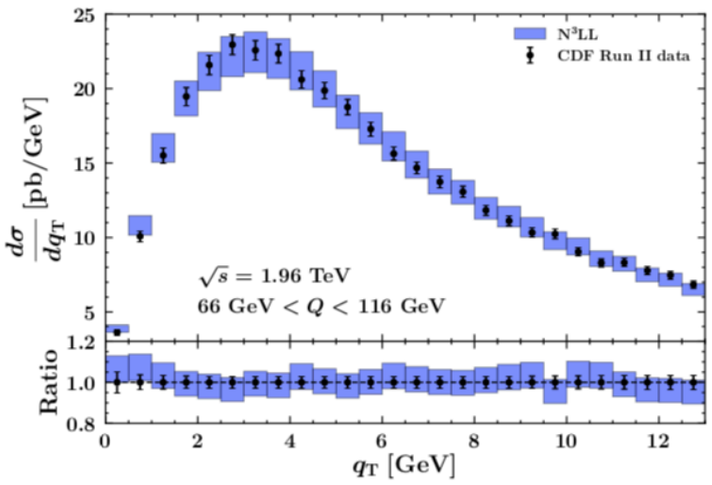

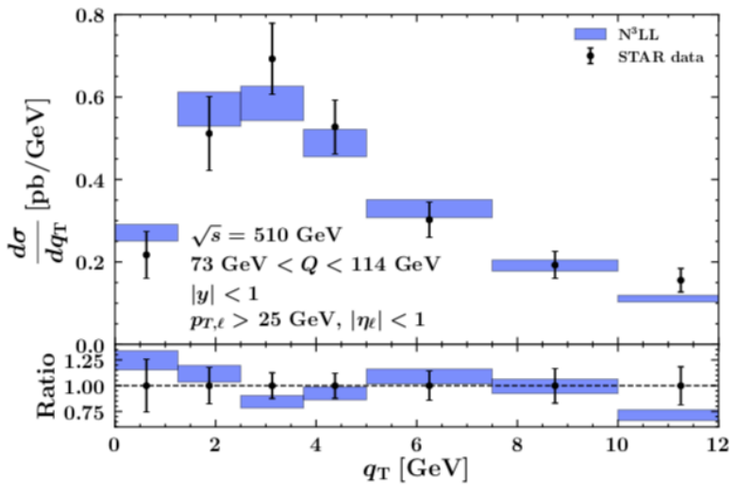

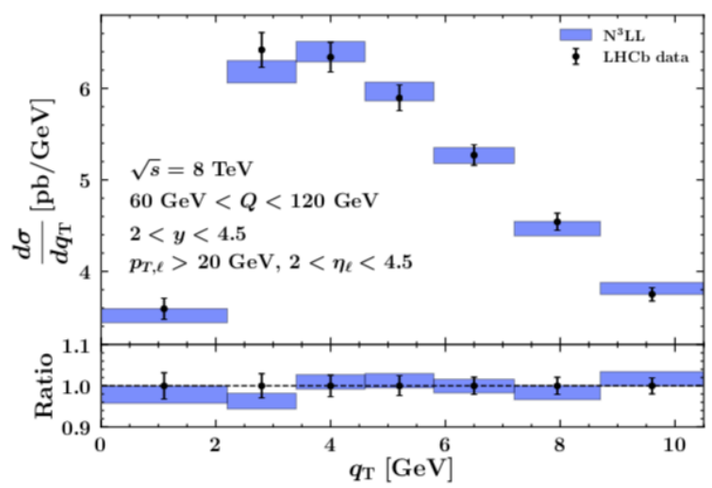

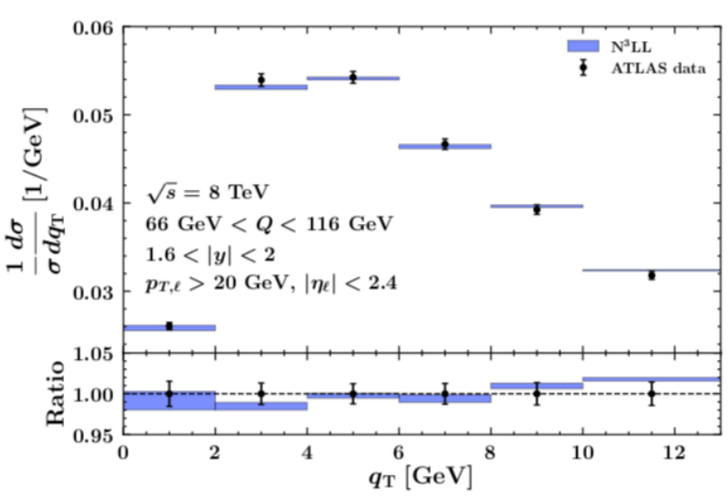

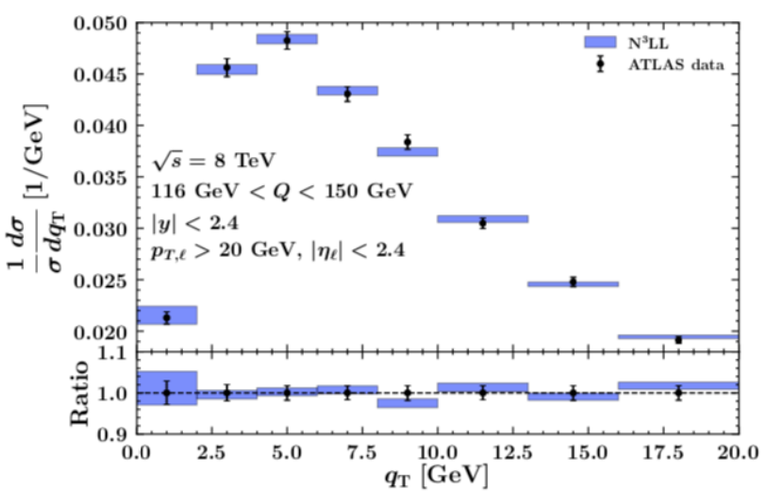

Experiment		$\chi^2_D/N_{\rm dat}$	$\chi^2_\lambda/N_{\rm dat}$	$\chi^2/N_{\rm dat}$
E605	7 GeV $< Q <$ 8 GeV	0.419	0.068	0.487
	8 GeV $< Q <$ 9 GeV	0.995	0.034	1.029
	10.5 GeV $< Q <$ 11.5 GeV	0.191	0.137	0.328
	11.5 GeV $< Q <$ 13.5 GeV	0.491	0.284	0.775
	13.5 GeV $< Q <$ 18 GeV	0.491	0.385	0.877
E288 200 GeV	4 GeV $< Q <$ 5 GeV	0.213	0.649	0.862
	5 GeV $< Q <$ 6 GeV	0.673	0.292	0.965
	6 GeV $< Q <$ 7 GeV	0.133	0.141	0.275
	7 GeV $< Q <$ 8 GeV	0.254	0.014	0.268
	8 GeV $< Q <$ 9 GeV	0.652	0.024	0.676
E288 300 GeV	4 GeV $< Q <$ 5 GeV	0.231	0.555	0.785
	5 GeV $< Q <$ 6 GeV	0.502	0.204	0.706
	6 GeV $< Q <$ 7 GeV	0.315	0.063	0.378
	7 GeV $< Q <$ 8 GeV	0.056	0.030	0.086
	8 GeV $< Q <$ 9 GeV	0.530	0.017	0.547
	11 GeV $< Q <$ 12 GeV	1.047	0.167	1.215
E288 400 GeV	5 GeV $< Q <$ 6 GeV	0.312	0.065	0.377
	6 GeV $< Q <$ 7 GeV	0.100	0.005	0.105
	7 GeV $< Q <$ 8 GeV	0.018	0.011	0.029
	8 GeV $< Q <$ 9 GeV	0.437	0.039	0.477
	11 GeV $< Q <$ 12 GeV	0.637	0.036	0.673
	12 GeV $< Q <$ 13 GeV	0.788	0.028	0.816
	13 GeV $< Q <$ 14 GeV	1.064	0.044	1.107
STAR		0.782	0.054	0.836
CDF Run I		0.480	0.058	0.538
CDF Run II		0.959	0.001	0.959
D0 Run I		0.711	0.043	0.753
D0 Run II		1.325	0.612	1.937
D0 Run II (μ)		3.196	0.023	3.218
LHCb 7 TeV		1.069	0.194	1.263
LHCb 8 TeV		0.460	0.075	0.535
LHCb 13 TeV		0.735	0.020	0.755
CMS 7 TeV		2.131	0.000	2.131
CMS 8 TeV		1.405	0.007	1.412
ATLAS 7 TeV	$0 < \|y\| < 1$	2.581	0.028	2.609
	$1 < \|y\| < 2$	4.333	1.032	5.365
	$2 < \|y\| < 2.4$	3.561	0.378	3.939
ATLAS 8 TeV on-peak	$0 < \|y\| < 0.4$	1.924	0.337	2.262
	$0.4 < \|y\| < 0.8$	2.342	0.247	2.590
	$0.8 < \|y\| < 1.2$	0.917	0.061	0.978
	$1.2 < \|y\| < 1.6$	0.912	0.095	1.006
	$1.6 < \|y\| < 2$	0.721	0.092	0.814
	$2 < \|y\| < 2.4$	0.932	0.348	1.280
ATLAS 8 TeV off-peak	46 GeV $< Q <$ 66 GeV	2.138	0.745	2.883
	116 GeV $< Q <$ 150 GeV	0.501	0.003	0.504
Global		**0.88**	**0.14**	**1.02**

SV2019

Dataset

- Both DY and SIDIS data:
  - fixed-target low-energy DY,
  - PHENIX data,
  - LHC and Tevatron data,
  - HERMES and COMPASS,
  - 457 + 582 = 1039 data points.

DY $\quad \delta \equiv \dfrac{\langle q_T \rangle}{\langle Q \rangle} < 0.1 \qquad \delta < 0.25 \quad \text{if} \quad \delta^2 < \sigma$

Experiment	ref.	$\sqrt{s}$ [GeV]	Q [GeV]	y/x_F	fiducial region	$N_{\rm pt}$ after cuts
E288 (200)	[64]	19.4	4 - 9 in 1 GeV bins*	$0.1 < x_F < 0.7$	-	43
E288 (300)	[64]	23.8	4 - 12 in 1 GeV bins*	$-0.09 < x_F < 0.51$	-	53
E288 (400)	[64]	27.4	5 - 14 in 1 GeV bins*	$-0.27 < x_F < 0.33$	-	76
E605	[65]	38.8	7 - 18 in 5 bins*	$-0.1 < x_F < 0.2$	-	53
E772	[66]	38.8	5 - 15 in 8 bins*	$0.1 < x_F < 0.3$	-	35
PHENIX	[67]	200	4.8 - 8.2	$1.2 < y < 2.2$	-	3
CDF (run1)	[68]	1800	66 - 116	-	-	33
CDF (run2)	[69]	1960	66 - 116	-	-	39
D0 (run1)	[70]	1800	75 - 105	-	-	16
D0 (run2)	[71]	1960	70 - 110	-	-	8
D0 (run2)$_\mu$	[72]	1960	65 - 115	$\lvert y\rvert < 1.7$	$p_T > 15$ GeV $\lvert\eta\rvert < 1.7$	3
ATLAS (7TeV)	[45]	7000	66 - 116	$\lvert y\rvert < 1$ $1 < \lvert y\rvert < 2$ $2 < \lvert y\rvert < 2.4$	$p_T > 20$ GeV $\lvert\eta\rvert < 2.4$	15
ATLAS (8TeV)	[46]	8000	66 - 116	$\lvert y\rvert < 2.4$ in 6 bins	$p_T > 20$ GeV $\lvert\eta\rvert < 2.4$	30
ATLAS (8TeV)	[46]	8000	46 - 66	$\lvert y\rvert < 2.4$	$p_T > 20$ GeV $\lvert\eta\rvert < 2.4$	3
ATLAS (8TeV)	[46]	8000	116 - 150	$\lvert y\rvert < 2.4$	$p_T > 20$ GeV $\lvert\eta\rvert < 2.4$	7
CMS (7TeV)	[47]	7000	60 - 120	$\lvert y\rvert < 2.1$	$p_T > 20$ GeV $\lvert\eta\rvert < 2.1$	8
CMS (8TeV)	[48]	8000	60 - 120	$\lvert y\rvert < 2.1$	$p_T > 20$ GeV $\lvert\eta\rvert < 2.1$	8
LHCb (7TeV)	[73]	7000	60 - 120	$2 < y < 4.5$	$p_T > 20$ GeV $2 < \eta < 4.5$	8
LHCb (8TeV)	[74]	8000	60 - 120	$2 < y < 4.5$	$p_T > 20$ GeV $2 < \eta < 4.5$	7
LHCb (13TeV)	[75]	13000	60 - 120	$2 < y < 4.5$	$p_T > 20$ GeV $2 < \eta < 4.5$	9
Total						457

*Bins with $9 \lesssim Q \lesssim 11$ are omitted due to the Υ resonance.

SIDIS $\quad \langle Q \rangle \geq 2\text{GeV} \qquad \delta \equiv \dfrac{\langle q_T \rangle}{\langle Q \rangle} < 0.25$

Experiment	Reaction	ref.	Kinematics	$N_{\rm pt}$ after cuts
HERMES	$p \to \pi^+$	[58]	0.023<x<0.6 (6 bins) 0.2<z<0.8 (6 bins) 1.0<Q<$\sqrt{20}$GeV $W^2 > 10\text{GeV}^2$ 0.1<y<0.85	24
	$p \to \pi^-$			24
	$p \to K^+$			24
	$p \to K^-$			24
	$D \to \pi^+$			24
	$D \to \pi^-$			24
	$D \to K^+$			24
	$D \to K^-$			24
COMPASS	$d \to h^+$	[59]	0.003<x<0.4 (8 bins) 0.2<z<0.8 (4 bins) 1.0<Q$\simeq$ 9GeV (5 bins)	195
	$d \to h^-$			195
Total				582

SV2019

Kinematic coverage

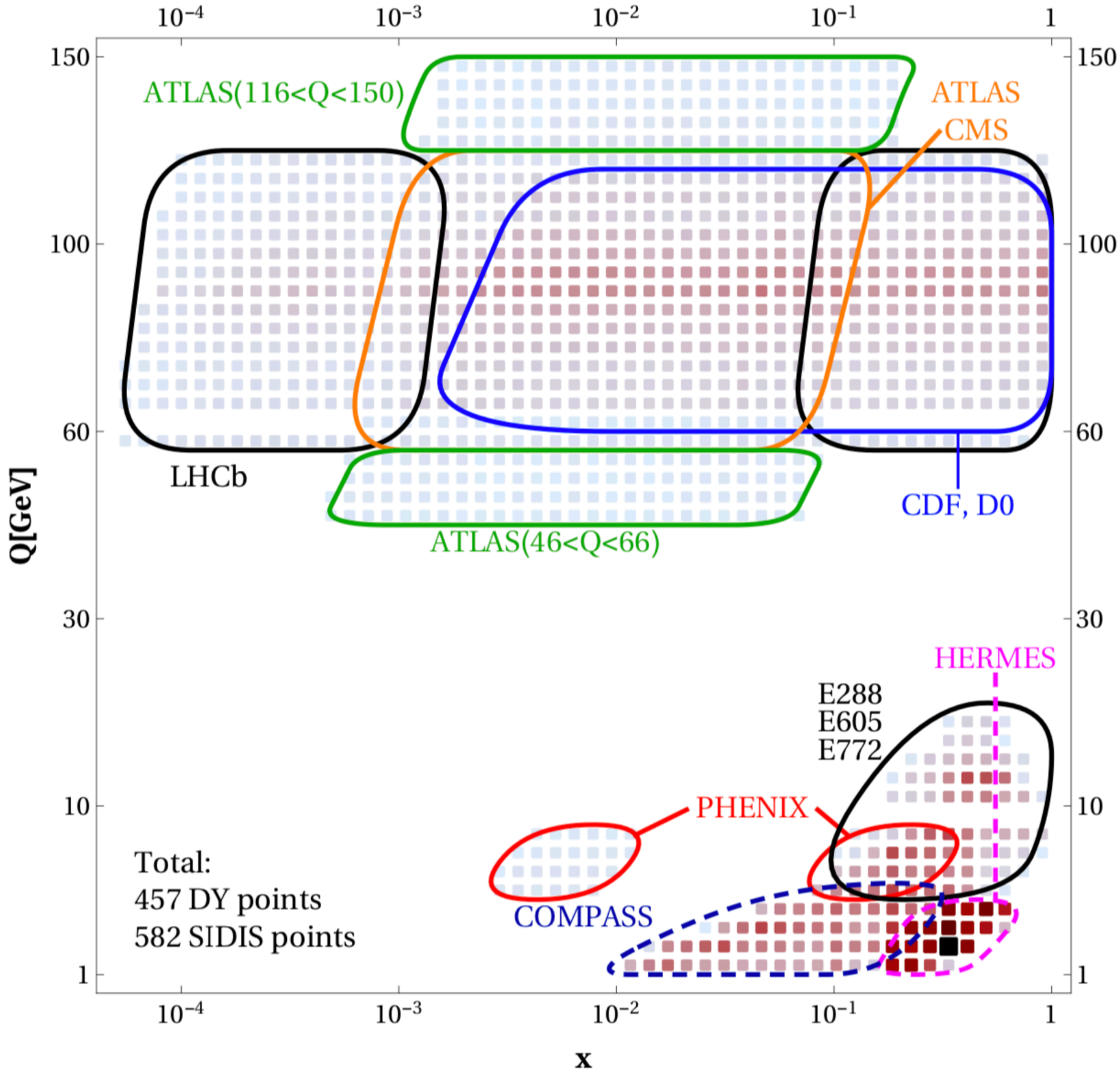

SV2019

Main settings

- b_* prescription: $$b_*(b_T) = \sqrt{\frac{b_T^2 B_{\rm NP}^2}{b_T^2 + B_{\rm NP}^2}}$$
- Non-perturbative function $f_{\rm NP}$:
  - evolution:
    $$g_K(b_T) = -c_0 b_T b_*(b_T) \quad \rightarrow \quad \begin{cases} -c_0 b_T^2 & \text{for } b_T \to 0 \\ -c_0 B_{\rm NP} b_T & \text{for } b_T \to \infty \end{cases}$$
  - PDFs and FFs:

$$f_{NP}(x,b) = \exp\left(-\frac{\lambda_1(1-x)+\lambda_2 x + x(1-x)\lambda_5}{\sqrt{1+\lambda_3 x^{\lambda_4}\boldsymbol{b}^2}}\boldsymbol{b}^2\right)$$

$$D_{NP}(x,b) = \exp\left(-\frac{\eta_1 z + \eta_2(1-z)}{\sqrt{1+\eta_3(\boldsymbol{b}/z)^2}}\frac{\boldsymbol{b}^2}{z^2}\right)\left(1+\eta_4\frac{\boldsymbol{b}^2}{z^2}\right)$$

- **11 free parameters** to fit to data.
- Perturbative accuracies: **NNLL'(NNLO), N³LL(-) (N³LO)**
- **Monte Carlo** method for the experimental error propagation.

SV2019

Fit quality

- Remarkably good total χ^2,
- DY and SIDIS data are separately well described,
- **Important achievement**:
  - simultaneous description of SIDIS and DY data within the same fit at high perturbative order.

		NNLO		N^{3}LO	
Data set	N_{pt}	χ^2/N_{pt}	$\langle d/\sigma \rangle$	χ^2/N_{pt}	$\langle d/\sigma \rangle$
CDF run1	33	0.66	8.4%	0.67	7.8%
CDF run2	39	1.28	2.8%	1.41	2.1%
D0 run1	16	0.72	0.1%	0.78	-0.5%
D0 run2	8	1.38	-	1.64	-
D0 run2 (μ)	3	0.62	-	0.69	-
Tevatron total	99	0.97		1.06	
ATLAS 7TeV 0.0<|y|<1.0	5	1.66	-	0.81	-
ATLAS 7TeV 1.0<|y|<2.0	5	5.94	-	4.09	-
ATLAS 7TeV 2.0<|y|<2.4	5	1.49	-	1.26	-
ATLAS 8TeV 0.0<|y|<0.4	5	2.51	3.5%	3.40	2.8%
ATLAS 8TeV 0.4<|y|<0.8	5	2.95	3.5%	3.03	2.7%
ATLAS 8TeV 0.8<|y|<1.2	5	1.30	3.7%	1.45	2.9%
ATLAS 8TeV 1.2<|y|<1.6	5	2.03	4.2%	1.53	3.4%
ATLAS 8TeV 1.6<|y|<2.0	5	1.47	4.9%	0.70	4.1%
ATLAS 8TeV 2.0<|y|<2.4	5	2.64	5.6%	2.10	4.8%
ATLAS 8TeV 46<Q<66GeV	3	0.31	1.1%	0.31	0.2%
ATLAS 8TeV 116<Q<150GeV	7	0.84	1.9%	0.97	1.2%
ATLAS total	55	2.12		1.82	
CMS 7TeV	8	1.25	-	1.24	-
CMS 8TeV	8	0.77	-	0.76	-
CMS total	16	1.01		1.00	
LHCb 7TeV	8	2.68	5.8%	2.37	5.2%
LHCb 8TeV	7	4.81	5.8%	4.16	5.1%
LHCb 13TeV	9	0.91	6.4%	0.81	5.7%
LHCb total	24	2.63		2.31	
High energy DY total	194	1.51		1.42	
PHE200	3	0.28	0.2%	0.29	-0.3%
E228-200	43	1.00	35.7%	1.12	35.0%
E228-300	53	0.90	29.2%	1.01	28.3%
E228-400	76	0.86	20.6%	0.96	19.5%
E772	35	1.84	9.5%	1.91	8.5%
E605	53	0.57	21.3%	0.60	20.1%
Low energy DY total	263	0.96		1.04	
HERMES ($p \to \pi^+$)	24	2.20	1.7%	3.06	2.2%
HERMES ($p \to \pi^-$)	24	1.12	0.6%	1.45	0.9%
HERMES ($p \to K^+$)	24	0.71	-0.1%	0.66	0.0%
HERMES ($p \to K^-$)	24	0.69	0.0%	0.66	0.0%
HERMES ($d \to \pi^+$)	24	0.57	0.3%	0.78	0.8%
HERMES ($d \to \pi^-$)	24	0.74	0.5%	0.96	0.7%
HERMES ($d \to K^+$)	24	0.52	-0.1%	0.53	0.0%
HERMES ($d \to K^-$)	24	1.27	0.0%	1.17	0.1%
HERMES total	192	0.98		1.16	
COMPASS ($d \to h^+$)	195	0.61	3.3%	0.76	5.1%
COMPASS ($d \to h^-$)	195	0.68	-2.3%	0.92	-0.5%
COMPASS total	390	0.65		0.84	
SIDIS total	582	0.76		0.95	
Total	**1039**	**0.95**		**1.06**	

SV2019

Fit quality

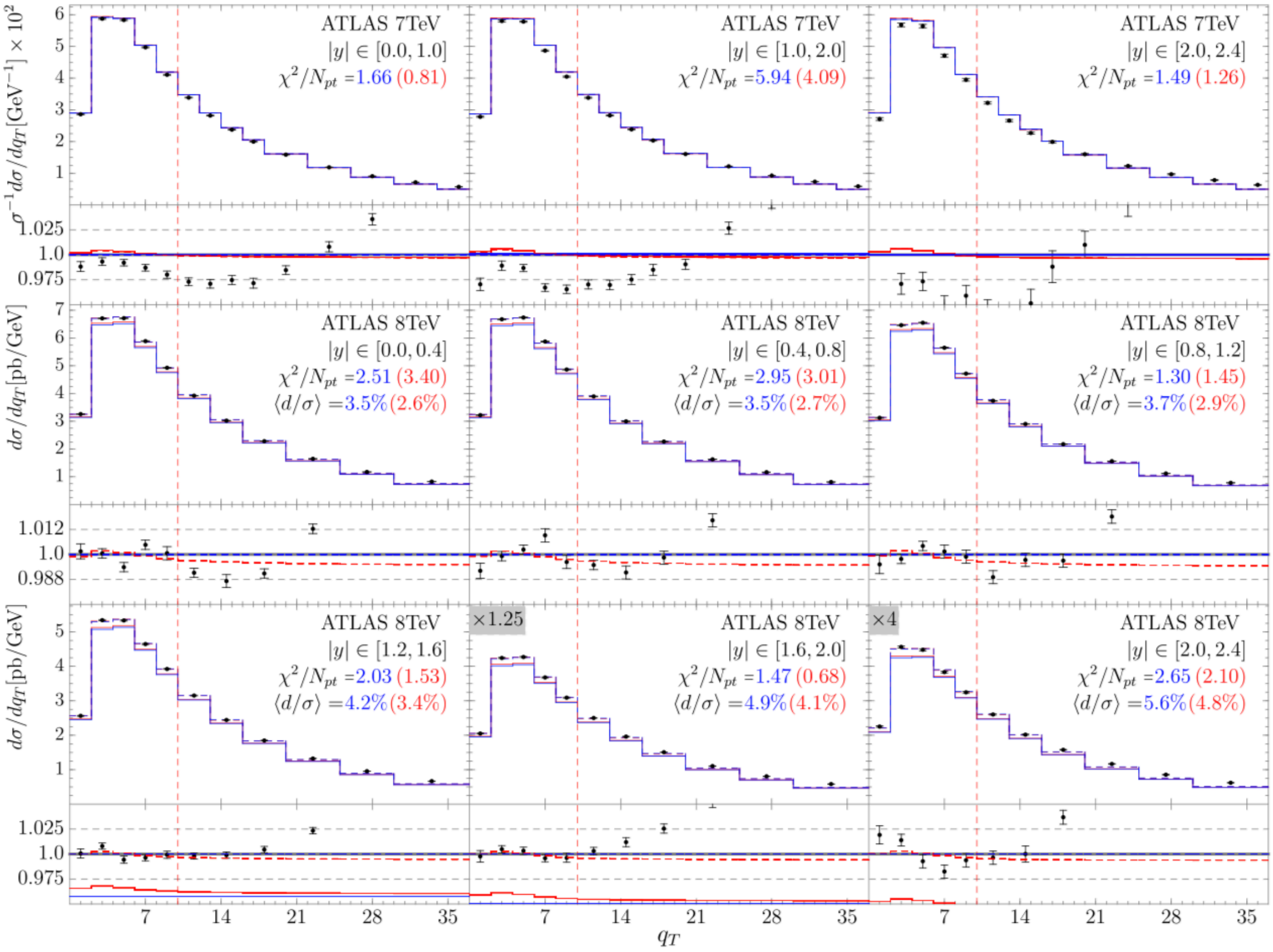

SV2019

Fit quality

$z^2 \times M(z, p_T)$

$d \to h^+$

COMPASS